Endosomal Chemokine Receptor Signalosomes Regulate Central Mechanisms Underlying Cell Migration

Hyunggu Hahn[1,2,*], Carole Daly[3,*], John Little IV[1,4*], Nicole A. Perry-Hauser[4,5], Asuka Inoue[6], Bianca Plouffe[3,#], Alex R. B. Thomsen[1,2,4,#].

[1]Department of Molecular Pathobiology, New York University College of Dentistry, New York, New York 10010, United States.
[2]NYU Pain Research Center, New York University College of Dentistry, New York, New York 10010, United States.
[3] Wellcome-Wolfson Institute for Experimental Medicine, Queen's University Belfast, Belfast, BT9 7BL, United Kingdom.
[4]Department of Surgery, Columbia University Columbia University Vagelos College of Physicians and Surgeons, New York, NY 10032, United States.
[5]Present affiliation: Departments of Psychiatry and Molecular Pharmacology and Therapeutics, Columbia University Vagelos College of Physicians and Surgeons, New York, NY 10032, USA
[6]Graduate School of Pharmaceutical Science, Tohoku University, Sendai, Miyagi 980-8578, Japan.

*Contributed equally and are co-first authors
[#]Corresponding authors

Abstract

Chemokine receptors are GPCRs that regulate chemotactic migration of a wide variety of cells including immune and cancer cells. Most chemokine receptors contain features associated with the ability to stimulate G proteins during β-arrestin-mediated internalization into endosomes. As endosomal signaling of certain non-GPCR receptors plays a major role in cell migration, we chose to investigate the potential role of endosomal chemokine receptor signaling on mechanisms governing this function. Applying cell biological approaches and spatiotemporal-resolved proteome profiling, we demonstrate that the model chemokine receptor CCR7 recruits G protein and β-arrestin simultaneously upon chemokine stimulation enabling internalized receptors to activate G protein from endosomes. Furthermore, endosomal CCR7 uniquely enriches specific Rho-GTPase regulators as compared to plasma membrane CCR7, which is associated with enhanced activity of Rho-GTPase Rac1. As Rac1 drives the formation of membrane protrusions during chemotaxis, our findings suggest an important integrated function of endosomal chemokine receptor signaling in cell migration.

Introduction

Chemokines are small proteins secreted from locations of physiological damage such as infection and inflammation. From these locations a gradient of chemokines is generated that attracts immune cells by activating their cell surface chemokine receptors, which triggers cell migration and differentiation to combat the pathophysiological state. The chemokine system is also taken advantage of by certain cancer cells including melanoma, glioblastoma, prostate, gastric, pancreatic, esophageal, ovarian, lung, colorectal, and breast cancer[1]. In malignant cells,

upregulation of chemokine receptors allows them to invade and metastasize to locations distinct from their origin and from where specific chemokines are secreted[1].

There exist 24 chemokine receptors that belong to the highly druggable superfamily of G protein-coupled receptors (GPCRs). Canonically, GPCRs activate heterotrimeric G proteins (Gαβγ) at the cell surface, causing downstream signaling throughout the cell[2]. This initial phase of G protein signaling is terminated via a specialized desensitization mechanism that includes phosphorylation of receptors by GPCR kinases and subsequent recruitment of β-arrestins (βarrs) to the phosphorylated receptor[3]. βarrs engage receptors at an overlapping transmembrane core region to where G proteins bind, and thus βarr recruitment to the receptor sterically blocks further G protein activation[4,5]. In addition, βarrs promote internalization of GPCRs into endosomes, thereby removing them from the source of the activating ligand[6].

Recent work has shown that some GPCRs continue to activate G proteins following βarr-mediated internalization into endosomes[7-12]. As G protein and βarr association to GPCRs have historically been considered mutually exclusive events, endosomal G protein signaling is difficult to reconcile within the general understanding of GPCR signaling. However, our recent work showed that certain GPCRs containing phosphorylation site clusters in their carboxy-terminal tail bind to βarrs in a specific conformation termed "tail conformation"[13]. In this conformation, βarr only interacts with the receptor carboxy-terminal tail thereby permitting the receptor transmembrane core to bind to G proteins simultaneously to form a "megaplex"[9,13,14]. Although formation of these GPCR–G protein–βarr megaplexes is not the only manner in which GPCRs activate G protein signaling from internalized compartments[10], the mechanism highlights how certain receptors that form strong association with βarrs can continue to stimulate G protein signaling over prolonged periods of time after they have been internalized into endosomes by βarrs.

Most chemokine receptors couple to similar G protein subtypes[15] and contain phosphorylation site clusters in their carboxy-terminal tail (Table S1), which raises the possibility that formation of megaplexes and endosomal G protein signaling are mechanisms applied by these receptors to influence physiological responses such as cell migration. Interestingly, endosomal signaling by other non-GPCR receptor systems such as receptor tyrosine kinases have a profound role in cell migration and control transport of various signaling complexes and other proteins between the cell surface and endosomal compartments during this process[16]. Therefore, our work here tests the hypothesis that chemokine receptors can stimulate G proteins from endosomes to regulate common signaling networks that direct cell migration.

Results

G protein signaling stimulated by CCR7 activation is not affected by βarr recruitment or βarr-mediated receptor endocytosis.

To study the potential role of megaplex and endosomal chemokine receptor signaling we used the model receptor CCR7. This receptor is an ideal model receptor to study endosomal signaling as it is activated by two endogenous chemokines CCL19 and CCL21; compared with the full agonist CCL19 that robustly stimulates $G_{i/o}$ signaling, receptor phosphorylation, βarr recruitment, and CCR7 internalization, the agonist CCL21 promotes full $G_{i/o}$ protein activation but only partial receptor phosphorylation and βarr recruitment, and minimal internalization of CCR7[17,18]. Using the real-time cAMP sensor CAMYEL[19] to monitor $G_{i/o}$ activity in HEK293 stably expressing CCR7 (HEK293-CCR7 cells), both CCL19 and CCL21 inhibited forskolin-induced cAMP production to a similar extent (Fig. 1A). This supports previous observations, which suggest that both CCL19 and CCL21 act as full agonists in stimulating $G_{i/o}$ signaling[17,18].

Interestingly, this $G_{i/o}$ signaling was sustained throughout the experiment and not acutely desensitized as other receptor systems such as the β_2-adrenergic receptor (Fig. 1A)[20]. Using the enhanced bystander bioluminescence resonance energy transfer (EbBRET)-based biosensors RlucII-βarr1/2 and cell surface-anchored rGFP-CAAX to monitor βarr1/2 recruitment to plasma membrane upon CCR7 stimulation (Fig. 1B)[21], we found that activating CCR7 by CCL19 leads to robust βarr1/2-recruitment, whereas CCL21 only promotes partial βarr1/2-recruitment responses (Fig. 1C-D). Co-expressing RlucII-βarr1/2 and the endosomally-located rGFP-Rab5 in HEK293-CCR7 cells, CCL19 stimulation leads to similar strong βarr1/2-mediated CCR7 internalization to endosomes whereas CCL21 stimulation of CCR7 only causes a minor translocation of βarr1/2 to the endosomes (Fig. 1B-D). These results suggest that CCR7 recruits and is internalized by βarrs robustly when stimulated with CCL19, but only to a modest degree by CCL21. Using β-galactosidase enzyme complementation-based DiscoveRx assays, we further confirmed that CCL19 strongly promotes βarr2 recruitment and βarr2-mediated CCR7 internalization, whereas CCL21 only promotes partial or insignificant βarr2-recruitment and βarr2-mediated receptor internalization, respectively (Fig. S1A-B).

Upon activation, CCR7 can complex with βarr1 in the tail conformation and engage with G_i protein and βarr1 simultaneously.

Surprisingly, neither the degree of βarr recruitment nor receptor internalization appear to affect CCR7-mediated G protein signaling as expected for most GPCRs. As we recently found a correlation between the presence of phosphorylation site clusters in GPCRs and their ability to form megaplexes[9], here we hypothesized that CCL19-CCR7 forms megaplexes and stimulates $G_{i/o}$ while being internalized into endosomes by βarrs (Fig. 2A). As numerous $G_{i/o}$-coupled GPCRs recently were demonstrated to form megaplexes, this hypothesis seems plausible[22]. In contrast, since CCL21 challenge only leads to minor CCR7 internalization, most of the CCL21-CCR7-mediated $G_{i/o}$ activation takes place at the plasma membrane (Fig. 2A).

For simultaneous GPCR association with G protein and βarr, βarrs need to complex exclusively through the phosphorylated receptor carboxy-terminal tail. We have previously demonstrated that other GPCRs with carboxy-terminal phosphorylation site clusters bind to βarrs in this tail conformation, and thus, it seemed likely that CCR7 could form them as well. To test this, we used a βarr1 mutant where the region of βarr1 that interacts with GPCR transmembrane cores, the fingerloop (FL), is deleted (βarr1-ΔFL). We showed previously using negative stain electron microscopy and single-particle averaging that βarr1-ΔFL almost entirely forms tail conformation complexes with GPCRs[13]. Using the EbBRET pair RlucII-βarr1-ΔFL and rGFP-CAAX (plasma membrane-anchored rGFP) in HEK293-CCR7 cells, we probed the degree of βarr1-ΔFL recruitment to CCR7 in response to CCL19, CCL21, or vehicle. In addition, we tested how well βarr1-ΔFL internalizes with CCR7 into endosomes using the EbBRET pair RlucII-βarr1-ΔFL and rGFP-Rab5 (early endosomes-anchored rGFP). Interestingly, both CCL19 and CCL21 stimulation led to recruitment of βarr1-ΔFL to CCR7 in the membrane although CCL19 promoted this recruitment to a significantly larger degree than CCL21 (Fig. 2B and S2). Furthermore, CCL19 and CCL21 stimulation promote βarr1-ΔFL translocation to endosomes (Fig. 2C and S2). These results indicate that CCR7 can form tail conformation complexes with βarr1 in cells and that the stability of this complex is sufficiently strong for βarr1 to internalize the receptor into endosomes.

Since CCR7 forms tail conformation complexes with βarr1 upon agonist stimulation where the G protein binding site is available, we next sought to interrogate whether the receptor binds to

βarrs and $G_{i/o}$ simultaneously to form a CCR7–$G_{i/o}$–βarr megaplex (Fig. 2D). To do this, we used a split NanoLuc (or NanoBiT) approach where the small-BiT (SmBiT) is fused to βarr1 and the large-BiT (LgBiT) is fused to the Gα subunit. If CCR7 recruits G protein and βarr1 simultaneously, the SmBiT-βarr1 and LgBiT-G will come into close proximity and form a functional luciferase, which catalyzes the conversion of coelenterazine h resulting in emission of a bright luminescence signal. Instead of using the full-length Gα subunit for this approach as done previously[9], we used a truncated surrogate version commonly referred to as miniGi. MiniG proteins are engineered Gα subunits that have been developed for the major Gα subunit families (G_s, $G_{i/o}$, $G_{q/11}$, and $G_{12/13}$). Key modifications of these Gα subunits include: 1) a truncated N-terminal that deletes membrane anchors and Gβγ-binding surface; 2) deletion of the α-helical domain; 3) mutations that improve protein stability *in vitro*; and 4) a mutation in the C-terminal α5 helix that uncouples GPCR binding from nucleotide release, therefore stabilizing receptor–miniG protein complexes in the presence of guanine nucleotides[23,24]. These alterations also enable miniG proteins to report receptor activation in living cells by measuring their recruitment from the cytoplasm to GPCRs at different membrane compartments[23]. Such properties are also beneficial when monitoring simultaneous recruitment of SmBiT-βarr1 and LgBiT-miniG to GPCRs that takes place during megaplex formation. Since both probes are expressed in the cytosol where they randomly collide, simultaneous translocation to the same receptors in the cell membrane will lead to a very specific increase in luminescence. In contrast, using a wild-type full length Gα subunit and βarr NanoBiT probes, which are located at the plasma membrane and cytosol, respectively, recruitment of βarrs to the receptor could lead to potential bystander effects as a result of βarrs-translocation from the cytosol to the plasma membrane.

In HEK293-CCR7 cells expressing SmBiT-βarr1 and LgBiT-miniGi, CCL19-stimulation leads to a robust increase in luminescence (Fig. S3). This signal was specific for miniGi as stimulation of CCR7 in cells expressing SmBiT-βarr1 and LgBiT-miniGs led to a small decrease in luminescence (Fig. S3). This reduction in basal luminescence might be caused by a reduction of random collision between SmBiT-βarr1 and LgBiT-miniGs upon CCR7 stimulation where SmBiT-βarr1, but not LgBiT-miniGs, translocates to the plasma membrane. These results indicate that CCL19-stimulated CCR7 recruits $G_{i/o}$ and βarrs simultaneously to form a CCR7-$G_{i/o}$-βarr megaplex. Next, we compared the ability of CCL19 and CCL21 to form megaplexes. Interestingly, both CCL19 and CCL21 stimulated CCR7–miniGi–βarr1 megaplex formation, although CCL19 promoted formation of these complexes to a significantly larger degree than CCL21 (Fig. 2E).

Megaplexes have been described as a mechanism by which GPCRs that bind βarrs exceptionally well via the phosphorylated C-terminal tail can promote endosomal G protein signaling[9]. Therefore, we investigated whether megaplexes form in endosomes using confocal microscopy. For this purpose, CCR7-expressing HEK293 cells co-expressing βarr2-Strawberry and Halo-miniGi were stimulated with either CCL19 or CCL21 for 30 min whereafter the subcellular location of these two probes was assessed by confocal microscopy. In this setup, only CCL19-CCR7 recruited βarr2-Strawberry and GFP-miniGi to endosomal-shaped intracellular locations whereas CCL21 did not (Fig. 2F-G). Together, these results indicate that CCL19 stimulation leads to robust endosomal CCR7–$G_{i/o}$–βarr1 megaplex formation.

Stimulation of CCR7 by CCL19, but not CCL21, leads to activation of $G_{i/o}$ signaling from endosomes.

To activate G protein from endosomes, CCR7 must internalize into endosomes while being bound to the non-permeable chemokine ligand. To investigate this potential event, we stimulated HEK-CCR7 cells that had been transfected with the early endosomal marker Rab5a-RFP with His-tagged CCL19 or CCL21. Before adding the chemokines, they were pre-coupled to Ni^{2+}-NTA-Alexa488 (CCL19/CCL21-Alexa488), and thus, their cellular location could be followed by confocal microscopy. After 15 min of stimulation, the CCL19/CCL21-Alexa488 present in the extracellular media was removed and the cells were washed twice with HBSS imaging buffer to remove any remaining extracellular-located chemokines. Hereafter, the cells were placed in culture media and potential wash-resistant internalized CCL19/CCL21-Alexa488 were monitored for 15-30 minutes after the washes by confocal microscopy. Substantial CCL19-Alexa488 internalized into distinct puncta that colocalize with Rab5a-RFP (Fig. 3A). In contrast, only negligible amounts of internalized Alexa488 were observed within the cells after the ligand washout steps of either CCL21-Alexa488 or Nickel-NTA-Alexa488 alone (Fig. 3A). These results indicate that CCR7 stimulation with CCL19, but not CCL21, indeed leads to prolonged internalization of CCL19-CCR7 into endosomes.

To test whether the internalized CCL19-CCR7 stimulates $G_{i/o}$ from internalized compartments, we measured translocation of RlucII-miniGi protein to the early endosomal marker rGFP-Rab5a by EbBRET in response to CCR7 challenge (Fig. 3B). Using this approach, CCL19 stimulation led to a strong and significant increase in EbBRET signaling between RlucII-miniGi and rGFP-Rab5a indicating that CCL19-bound CCR7 indeed activates $G_{i/o}$ from endosomes (Fig. 3C). In contrast, CCL21 stimulation provoked a small and insignificant increase of EbBRET response, demonstrating that little to no $G_{i/o}$ protein is activated from endosomes by CCL21-bound CCR7 (Fig. 3C). This trend was also observed by confocal microscopy visualization of CCR7-expressing HEK293 co-expressing Halo-miniGi and either the plasma membrane marker RFP-Lck or the early endosomal marker RFP-EEA1. In these cells, activation by CCL19, but not CCL21, resulted in co-localization of miniGi and RFP-EEA1 at endosomes further indicating that CCL19-CCR7 promotes G protein activation from endosomes whereas CCL21-CCR7 predominantly activates $G_{i/o}$ at the cell surface (Fig. 3D-G).

APEX2-based proteome profiling demonstrates that CCR7 assembles distinct signalosomes upon stimulation with either CCL19 or CCL21.

Limited knowledge exists regarding functional outcomes of endosomal G protein signaling by internalized GPCRs, particularly chemokine receptors. Thus, to examine the impact of compartmentalized CCR7 signaling on downstream effectors, we performed unbiased mass spectrometry (MS)-based proteome profiling using APEX2. APEX2 is an engineered ascorbate peroxidase enzyme that we fused to the CCR7 carboxy-terminal and uses H_2O_2 as an oxidant to catalyze a one electron oxidation of various small molecule substrates including biotin-tyramide (Fig. 4A). Oxidation of biotin-tyramide leads to generation of a highly reactive and short-lived (<1 ms) biotin-phenoxyl radical that conjugates to endogenous proteins that are in close proximity to the APEX2 enzyme (~20 nm, Fig. 4A)[25]. Thus, the APEX2 application allows for spatiotemporal control of the biotinylation process with high precision. The resulting biotinylated proteins are then enriched with pull-down experiments using neutravidin beads, and their identities analyzed by MS (Fig. 4A).

Receptor functionality of the CCR7-APEX2 construct was confirmed by assessing its ability to inhibit forskolin-induced cAMP production in response to CCL19 stimulation (Fig. S4). In addition, we verified that the APEX2 portion of fusion proteins only biotinylates proteins in the

presence of both biotin-tyramide and hydrogen peroxide as expected (Fig. 4B). Using neutravidin beads, we demonstrated that proteins were pulled-down from HEK293-CCR7-APEX2 cell lysates where the biotinylation process had been initiated, whereas only negligible proteins were pulled-down in untreated cells (Fig. 4C). Together these results indicate that both receptor and APEX2's enzyme functions of the CCR7-APEX2 fusion are intact.

Using our experimental setup, we stimulated HEK293-CCR7-APEX2 cells pretreated with biotin-tyramide with either CCL19 or CCL21 for 0 minute, 2 minutes, 10 minutes or 25 minutes. Hereafter, the biotinylation reaction was initiated by addition of hydrogen peroxide for exactly 1 min, followed by extensive washing, cell lysis, enrichment of biotinylated proteins, and MS profiling.

From the MS profiling we identified a total of 579 proteins, whose enrichment was changed significantly ($p < 0.05$ and change in intensity of $\log_2 > 1$) (Fig. S5). Among robustly enriched proteins by CCR7 activation, several are involved in functions related to vesicle trafficking, signal transduction, cytoskeletal dynamics, and cell migration among others (Fig. 5A). Furthermore, as CCR7 is trafficked from the plasma membrane to endosomes within the first 10 min of stimulation, we also included functionally validated APEX2-fused spatial references, PM-APEX2, ENDO-APEX2, and CYTO-APEX2 to control for the potential increase in random collisions between CCR7 and endosomal proteins that might occur upon receptor internalization (Fig. 5B-D and S6)[26]. Proteins enriched by both ENDO-APEX2 (as compared to both CYTO-APEX2 and PM-APEX2) and chemokine-stimulated CCR7-APEX2 include SNX3, RAB9A, ARH, and CCD93 (Fig. 5A and 5D). Thus, these proteins might be enriched by CCR7-APEX2 due to chemokine-stimulated translocation from the plasma membrane to endosomes rather than participating in multiprotein functional complexes or 'signalosomes' forming at CCR7.

As expected, proteins involved in receptor and vesicular trafficking including RIC, SNX17, VA0D1, ARRB2, and DYN3, among others, were enriched over the entire time course of CCR7 activation (Fig. 5A). Most of these proteins were more enriched by CCL19 stimulation as compared to CCL21 challenge. In addition, we observed enrichment of endosomal proteins such as STX7, STX12, and VTI1B for both CCL19 and CCL21 stimulation (Fig. 5A). Interestingly, the lysosomal marker LAMP1 was enriched by CCL19 and to a lesser degree by CCL21 after 25 minutes of stimulation (Fig. 5A). Proteins involved in receptor recycling such as SNX6, RAB7L, and GGA3 were also enriched at the later stages of CCR7 activation particularly when stimulated with CCL21 (Fig. 5A). These results indicate that the trafficking pattern of CCR7 upon chemokine stimulation is tightly regulated between lysosomal degradation and endosomal recycling.

Among enriched signaling proteins, we observed robust enrichment of proteins regulating inositol 1,4,5-triphosphate signaling (ERLN1/2, IP3KA), diacyl glycerol signaling (DGKQ), calcium mobilization at the endoplasmic reticulum (TMCO1), and activity of the Rho-GTPases (Fig. 5A and 5E-G). These are all involved in signaling events downstream of heterotrimeric G protein activation. Another interesting signaling protein enriched by CCR7 activation includes members of the eyes absent (EYA) subfamily of proteins, EYA2. These proteins have been shown to interact with and regulate Gαi and Gαz subunits[27,28], and EYA4, a member of the same family, was recently identified in a similar APEX2-based study of the μ-opioid receptor[29]. We also detected three novel interaction partners GRIP2, MARK4, and EI24 as being among the highest levels regardless of the activation ligand or time (Fig 5A and S5B).

Endosomal $G_{i/o}$ signaling as an important foundation for cell migratory Rac1 activation.

Rho-GTPases such as RhoA, Rac1, Cdc42 regulate important aspects of chemotactic cell migration[30]. Activity of these effectors are regulated by other proteins such as Rho-GTPase-activating proteins (GAPs), Rho guanine nucleotide exchange factors (GEFs), and Rho GDP dissociation inhibitors (GDIs) (Fig. 5E). Our APEX2-based proteomics results demonstrate that a number of these Rho-GTPase regulators are enriched by chemokine-stimulation of CCR7, and thus, potentially form part of larger CCR7 signalosomes that control downstream Rho-GTPase activity (Fig. 5F and 5G). Interestingly, some of these regulators, including RHG26, ARG28, RHG29, ACK1, and BORG5, were differentially enriched upon CCL19 or CCL21 stimulation (Fig. 5F). Therefore, it is possible that CCR7 signaling modulates activity of cell migratory Rho-GTPases specifically at distinct cellular locations. To test this hypothesis, we focused on RhoA, Rac1, and Cdc42. Upon activation of RhoA, Rac1, and Cdc42, they recruit protein kinase N1 (PKN1), p21 activated kinase 1 (PAK1), and Wiskott-Aldrich syndrome protein 1 (WAS1), respectively. We assessed the proximity of these biosensor pairs in real-time upon chemokine stimulation by the NanoBiT approach in HEK293-CCR7 cells (Fig. 6A). Using this setup, we found that both CCL19 and CCL21 stimulated RhoA and Cdc42 activation to a similar extent, which indicates that the spatial aspect of G protein activation does not appear to influence RhoA and Cdc42 signaling (Fig. 6B and 6D). In contrast, CCL19 promoted Rac1 signaling to a significantly greater extent than CCL21 stimulation (Fig. 6C). Pre-incubating the cells with the $G_{i/o}$ inhibitor pertussis toxin (PTX), virtually eliminated the chemokine-induced activation of Rac1, indicating that CCR7-stimulateted Rac1 signaling is mediated via a $G_{i/o}$-dependent mechanism (Fig. 6E). Interestingly, preincubation of the HEK293-CCR7 cells with the endocytosis inhibitor Dyngo-4a[7] reduced chemokine Rac1 activation robustly (Fig. 6F). This reduction was significantly smaller as compared to cells pre-incubated with an inactive Dyngo compound[7], suggesting that CCR7-mediated Rac1 activation depends on receptor internalization (Fig. 6F). Together, these results provide a strong basis for endosomal $G_{i/o}$ signaling by internalized CCR7 as a mechanism to activate Rac1.

Discussion

Historically, GPCRs have been thought to activate heterotrimeric G proteins exclusively from the cell surface, which leads to downstream signaling events that regulate cell physiological responses. This G protein signaling has been characterized as short-lived due to a specialized desensitization mechanism that includes receptor phosphorylation by GPCR kinases and subsequent recruitment of βarrs to the phosphorylated receptor. The GPCR–βarr interaction both uncouples G protein from the receptor and promotes receptor endocytosis, which are hallmarks of receptor desensitization.

This paradigm, however, has been challenged over the past 10-15 years by multiple observations, which show GPCRs that continue to activate G proteins from internalized compartments, such as from endosomes. Paradoxically, GPCRs that promote endosomal G protein signaling most substantially include receptors such as the vasopressin type 2 receptor (V_2R), parathyroid hormone receptor 1, protease-activated receptor type 2, and neurokinin 1 receptor that all associate strongly with βarrs via phosphorylation site clusters located at their carboxy-terminal tail[7,9,12,31,32]. Recently, we demonstrated that GPCRs with these carboxy-terminal clusters associate with βarrs exclusively through this region to form tail conformation GPCR–βarr complexes[13]. Since βarrs do not block the G protein-binding site in this tail conformation, the receptor can associate with βarrs and G proteins simultaneously to form GPCR–G protein–βarr

'megaplexes'[9,14]. The assembly of these megaplexes allows the receptor to continue to stimulate G protein signaling while being internalized into endosomes by βarrs.

The chemokine receptor CCR7 contains serine/threonine phosphorylation site clusters on its carboxy-terminal tail (Table S1), which have been shown to be fully phosphorylated upon CCL19 stimulation, but not CCL21 stimulation[17,18]. In the present study, we found a correlation between this reported CCR7 phosphorylation pattern, formation of tail conformation CCR7–βarr1 complexes, simultaneous recruitment of G protein and βarr to form CCR7–$G_{i/o}$–βarr1 megaplexes, and robust endosomal G protein signaling (Figs. 1-3). As most chemokine receptors also contain these serine/threonine phosphorylation site clusters in their carboxy-terminal tails, it not only raises the possibility that these receptors can promote endosomal G protein signaling, but also that this mode of signaling regulates important aspects of the physiological functions associated with these receptors (Table S1). In fact, removing the carboxy-terminal tail or mutating its phosphorylation sites in the chemokine receptors CXCR1-4 reduces their ability to internalize and promote cellular chemotaxis towards a chemokine-gradient[33-35]. Similar reduction in chemotaxis of immune cells towards gradients of different chemokines was observed upon pharmacological inhibition of endocytosis[36]. Additionally, removal of intracellular loops in CXCR4 reduces G protein activation and is associated with decreased capacity of CXCR4 to promote cell migration indicating a co-dependency of G protein signaling and receptor internalization on this cell physiological function[33]. Notably, the chemokine receptor CCR1 displays constitutive G protein activation and internalization in HEK293 cells by a mechanism where Gαi and βarr complex with the receptor simultaneously[37]. This constitutive CCR1-mediated G protein activation from internalized compartment was reported to stimulate cell migration. Finally, sustained $G_{i/o}$ signaling by internalized sphingosine-1-phophate type 1 receptor has been shown to promote cell migration in human umbilical vein endothelial cells[38]. Thus, previous observations are supportive of certain aspects of cell migration being regulated by internalized chemokine receptor signaling.

To obtain a greater understanding of the impact of endosomal chemokine receptor signaling on cell physiological responses, we applied an unbiased MS-based proteome profiling approach using CCR7-APEX2 expressing HEK293 cells. We found that CCR7 activation leads to enrichment of multiple proteins of key functions including vesicle trafficking, signal transduction, and cytoskeletal dynamics/cell migratory, among others (Fig. 5A). The proteins GRIP2 and EI24 were among the most enriched following CCR7 activation. GRIP2 and EI24 have not previously been reported as having roles in GPCR biology. GRIP2 has been shown to bind AMPA ionotropic glutamate receptors via PDZ-domains to regulate their intracellular trafficking[39,40]. Whether GRIP2 plays similar role in the trafficking of chemokine receptors remains to be tested. EI24 is a protein whose expression is enhanced by p53 activation, and plays a role in in growth suppression and apoptosis as well as in autophagy through formation of degradative autolysosomes[41]. As with GRIP2, the potential role of EI24 in chemokine receptor biology is unknown. Another highly enriched protein was cytosolic EYA2, which interacts with members of the *Sine oculis* (Six) family of homeodomain transcription factors. This interaction facilitates the translocation of EYA proteins into the nucleus, where the EYA/Six complex regulates transcription of a number of genes involved in development and cancer[42]. Interestingly, EYA2 can interact directly with Gαi and Gαz subunits and regulate their activity[27,28]. This interaction prevents their translocation to the nucleus, and thus, block their role as transcription co-factors[27]. Coincidently, EYA4 was recently identified in a similar APEX2-based study of the μ-opioid receptor, and thus, might be more involved in downstream signaling responses of G_i-coupled receptors such as chemokine receptors than currently appreciated[29].

Another protein that was robustly enriched upon CCR7-APEX2 activation was the Rho-GTPase GAP RHG26. Notably, this enrichment was exclusively observed when HEK293-CCR7-APEX2 cells were stimulated by CCL19, but not CCL21 (Fig. 5A and 5F). Other regulators of Rho-GTPases were also enriched by CCR7 activation and some of them were differentially enriched by either CCL19 or CCL21 stimulation (Fig. 5F). These results raise the possibility that compartmentalized CCR7 signaling could play an important role in downstream Rho-GTPase activity. In fact, we discovered that the Rho-GTPase Rac1 was specifically activated by endosomal G protein signaling by internalized CCR7 whereas the Rho-GTPases RhoA and Cdc42 were stimulated equally by plasma membrane and endosomal CCR7 signaling (Fig. 6). Rac1 plays a key role in cell migration, and can be activated in endosomes by the RhoGEF Tiam1 and Vav1[16,43]. This activation leads to Rac1 translocation to the cell surface via recycling endosomes, a process reported to occur in response to stimulation of CCR7 as well as several receptor tyrosine kinases[16,43]. From this subcellular region, Rac1 activates the major effector PAK1, which phosphorylates LIM kinase and cortactin, among others, to coordinate actin polymerization at the plasma membrane region[44]. This polymerization leads to formation of cytoskeletal actin filaments that serve as underlying stabilizing structures of newly formed filopodia and lamellipodia[44]. As these membrane protrusions constitute a major mechanistic step during cell migration, endosomal Rac1 activation plays a central role in this cell physiological process[30]. To this end, CCL19 has been reported to trigger cell migration more robustly and with greater potency as compared to CCL21 despite both chemokines activating CCR7 with similar affinities[18,45-47]. Thus, the findings from our study highlight the formation of megaplexes and stimulation of endosomal G protein signaling by chemokine receptors as a potential general mechanism that regulates key aspects of cell migration.

Acknowledgments

We are grateful to Dr. Nigel Bunnett for fruitful discussions and generous gift of the plasmid encoding the CAMYEL cAMP biosensor. We thank Dr. Mark von Zastrow for the generous gifts of the plasmids encoding PM-APEX2, ENDO-APEX2, and CYTO-APEX2. We are also grateful for support by and discussions with Evgeny Kanshin and Beatrix Ueberheide at NYU School of Medicine Proteomics Laboratory. This work received support from the LEO Foundation (LF18043 to A.R.B.T.), NIH grants (R35GM147088 (NIGMS) and R21CA243052 (NCI) to A.R.B.T.), and a Wellcome Trust Seed Award (215229/Z/19/Z to B.P.). A.I. was funded by Japan Society for the Promotion of Science (JSPS) KAKENHI grants 21H04791, 21H05113, JPJSBP120213501 and JPJSBP120218801; FOREST Program JPMJFR215T and JST Moonshot Research and Development Program JPMJMS2023 from Japan Science and Technology Agency (JST); The Uehara Memorial Foundation; and Daiichi Sankyo Foundation of Life Science.

References

1 Sarvaiya, P. J., Guo, D., Ulasov, I., Gabikian, P. & Lesniak, M. S. Chemokines in tumor progression and metastasis. *Oncotarget* **4**, 2171-2185, doi:10.18632/oncotarget.1426 (2013).

2 Gilman, A. G. G proteins: transducers of receptor-generated signals. *Annu Rev Biochem* **56**, 615-649, doi:10.1146/annurev.bi.56.070187.003151 (1987).

3 Moore, C. A., Milano, S. K. & Benovic, J. L. Regulation of receptor trafficking by GRKs and arrestins. *Annu Rev Physiol* **69**, 451-482, doi:10.1146/annurev.physiol.69.022405.154712 (2007).

4 Lohse, M. J., Benovic, J. L., Codina, J., Caron, M. G. & Lefkowitz, R. J. beta-Arrestin: a protein that regulates beta-adrenergic receptor function. *Science* **248**, 1547-1550, doi:10.1126/science.2163110 (1990).

5 Lee, Y. *et al.* Molecular basis of beta-arrestin coupling to formoterol-bound beta1-adrenoceptor. *Nature* **583**, 862-866, doi:10.1038/s41586-020-2419-1 (2020).

6 Goodman, O. B., Jr. *et al.* Beta-arrestin acts as a clathrin adaptor in endocytosis of the beta2-adrenergic receptor. *Nature* **383**, 447-450, doi:10.1038/383447a0 (1996).

7 Jensen, D. D. *et al.* Neurokinin 1 receptor signaling in endosomes mediates sustained nociception and is a viable therapeutic target for prolonged pain relief. *Sci Transl Med* **9**, doi:10.1126/scitranslmed.aal3447 (2017).

8 Thomsen, A. R. B., Jensen, D. D., Hicks, G. A. & Bunnett, N. W. Therapeutic Targeting of Endosomal G-Protein-Coupled Receptors. *Trends Pharmacol Sci* **39**, 879-891, doi:10.1016/j.tips.2018.08.003 (2018).

9 Thomsen, A. R. B. *et al.* GPCR-G Protein-beta-Arrestin Super-Complex Mediates Sustained G Protein Signaling. *Cell* **166**, 907-919, doi:10.1016/j.cell.2016.07.004 (2016).

10 Irannejad, R. *et al.* Conformational biosensors reveal GPCR signalling from endosomes. *Nature* **495**, 534-538, doi:10.1038/nature12000 (2013).

11 Calebiro, D. *et al.* Persistent cAMP-signals triggered by internalized G-protein-coupled receptors. *PLoS Biol* **7**, e1000172, doi:10.1371/journal.pbio.1000172 (2009).

12 Wehbi, V. L. *et al.* Noncanonical GPCR signaling arising from a PTH receptor-arrestin-Gbetagamma complex. *Proc Natl Acad Sci U S A* **110**, 1530-1535, doi:10.1073/pnas.1205756110 (2013).

13 Cahill, T. J., 3rd *et al.* Distinct conformations of GPCR-beta-arrestin complexes mediate desensitization, signaling, and endocytosis. *Proc Natl Acad Sci U S A* **114**, 2562-2567, doi:10.1073/pnas.1701529114 (2017).

14 Nguyen, A. H. *et al.* Structure of an endosomal signaling GPCR-G protein-beta-arrestin megacomplex. *Nat Struct Mol Biol* **26**, 1123-1131, doi:10.1038/s41594-019-0330-y (2019).

15 Hughes, C. E. & Nibbs, R. J. B. A guide to chemokines and their receptors. *FEBS J* **285**, 2944-2971, doi:10.1111/febs.14466 (2018).

16 Palamidessi, A. *et al.* Endocytic trafficking of Rac is required for the spatial restriction of signaling in cell migration. *Cell* **134**, 135-147, doi:10.1016/j.cell.2008.05.034 (2008).

17 Zidar, D. A., Violin, J. D., Whalen, E. J. & Lefkowitz, R. J. Selective engagement of G protein coupled receptor kinases (GRKs) encodes distinct functions of biased ligands. *Proc Natl Acad Sci U S A* **106**, 9649-9654, doi:10.1073/pnas.0904361106 (2009).

18 Kohout, T. A. *et al.* Differential desensitization, receptor phosphorylation, beta-arrestin recruitment, and ERK1/2 activation by the two endogenous ligands for the CC chemokine receptor 7. *J Biol Chem* **279**, 23214-23222, doi:10.1074/jbc.M402125200 (2004).

19 Jiang, L. I. *et al.* Use of a cAMP BRET sensor to characterize a novel regulation of cAMP by the sphingosine 1-phosphate/G13 pathway. *J Biol Chem* **282**, 10576-10584, doi:10.1074/jbc.M609695200 (2007).

20 Violin, J. D. *et al.* beta2-adrenergic receptor signaling and desensitization elucidated by quantitative modeling of real time cAMP dynamics. *J Biol Chem* **283**, 2949-2961, doi:10.1074/jbc.M707009200 (2008).
21 Namkung, Y. *et al.* Monitoring G protein-coupled receptor and beta-arrestin trafficking in live cells using enhanced bystander BRET. *Nat Commun* **7**, 12178, doi:10.1038/ncomms12178 (2016).
22 Smith, J. S. *et al.* Noncanonical scaffolding of Galphai and beta-arrestin by G protein-coupled receptors. *Science* **371**, doi:10.1126/science.aay1833 (2021).
23 Wan, Q. *et al.* Mini G protein probes for active G protein-coupled receptors (GPCRs) in live cells. *J Biol Chem* **293**, 7466-7473, doi:10.1074/jbc.RA118.001975 (2018).
24 Nehme, R. *et al.* Mini-G proteins: Novel tools for studying GPCRs in their active conformation. *PLoS One* **12**, e0175642, doi:10.1371/journal.pone.0175642 (2017).
25 Tan, B. *et al.* An Optimized Protocol for Proximity Biotinylation in Confluent Epithelial Cell Cultures Using the Peroxidase APEX2. *STAR Protoc* **1**, 100074, doi:10.1016/j.xpro.2020.100074 (2020).
26 Lobingier, B. T. *et al.* An Approach to Spatiotemporally Resolve Protein Interaction Networks in Living Cells. *Cell* **169**, 350-360 e312, doi:10.1016/j.cell.2017.03.022 (2017).
27 Embry, A. C., Glick, J. L., Linder, M. E. & Casey, P. J. Reciprocal signaling between the transcriptional co-factor Eya2 and specific members of the Galphai family. *Mol Pharmacol* **66**, 1325-1331, doi:10.1124/mol.104.004093 (2004).
28 Fan, X. *et al.* The alpha subunits of Gz and Gi interact with the eyes absent transcription cofactor Eya2, preventing its interaction with the six class of homeodomain-containing proteins. *J Biol Chem* **275**, 32129-32134, doi:10.1074/jbc.M004577200 (2000).
29 Polacco, B. J. L. B. T. B. E. E. A. N. X. J. L. Q. N. Z. Z. C. S. B. Profiling the diversity of agonist-selective effects on the proximal proteome environment of G protein-coupled receptors.
BioRxiv, doi:https://doi.org/10.1101/2022.03.28.486115 (2022).
30 Schiefermeier, N., Teis, D. & Huber, L. A. Endosomal signaling and cell migration. *Curr Opin Cell Biol* **23**, 615-620, doi:10.1016/j.ceb.2011.04.001 (2011).
31 Feinstein, T. N. *et al.* Noncanonical control of vasopressin receptor type 2 signaling by retromer and arrestin. *J Biol Chem* **288**, 27849-27860, doi:10.1074/jbc.M112.445098 (2013).
32 Jimenez-Vargas, N. N. *et al.* Protease-activated receptor-2 in endosomes signals persistent pain of irritable bowel syndrome. *Proc Natl Acad Sci U S A* **115**, E7438-E7447, doi:10.1073/pnas.1721891115 (2018).
33 Roland, J. *et al.* Role of the intracellular domains of CXCR4 in SDF-1-mediated signaling. *Blood* **101**, 399-406, doi:10.1182/blood-2002-03-0978 (2003).
34 Richardson, R. M., Marjoram, R. J., Barak, L. S. & Snyderman, R. Role of the cytoplasmic tails of CXCR1 and CXCR2 in mediating leukocyte migration, activation, and regulation. *J Immunol* **170**, 2904-2911, doi:10.4049/jimmunol.170.6.2904 (2003).
35 Colvin, R. A., Campanella, G. S., Sun, J. & Luster, A. D. Intracellular domains of CXCR3 that mediate CXCL9, CXCL10, and CXCL11 function. *J Biol Chem* **279**, 30219-30227, doi:10.1074/jbc.M403595200 (2004).
36 Jacques, R. O. *et al.* Dynamin function is important for chemokine receptor-induced cell migration. *Cell Biochem Funct* **33**, 407-414, doi:10.1002/cbf.3131 (2015).

37 Gilliland, C. T., Salanga, C. L., Kawamura, T., Trejo, J. & Handel, T. M. The chemokine receptor CCR1 is constitutively active, which leads to G protein-independent, beta-arrestin-mediated internalization. *J Biol Chem* **288**, 32194-32210, doi:10.1074/jbc.M113.503797 (2013).

38 Mullershausen, F. *et al.* Persistent signaling induced by FTY720-phosphate is mediated by internalized S1P1 receptors. *Nat Chem Biol* **5**, 428-434, doi:10.1038/nchembio.173 (2009).

39 Mao, L., Takamiya, K., Thomas, G., Lin, D. T. & Huganir, R. L. GRIP1 and 2 regulate activity-dependent AMPA receptor recycling via exocyst complex interactions. *Proc Natl Acad Sci U S A* **107**, 19038-19043, doi:10.1073/pnas.1013494107 (2010).

40 Dong, H. *et al.* Characterization of the glutamate receptor-interacting proteins GRIP1 and GRIP2. *J Neurosci* **19**, 6930-6941 (1999).

41 Tian, Y. *et al.* C. elegans screen identifies autophagy genes specific to multicellular organisms. *Cell* **141**, 1042-1055, doi:10.1016/j.cell.2010.04.034 (2010).

42 Tadjuidje, E. & Hegde, R. S. The Eyes Absent proteins in development and disease. *Cell Mol Life Sci* **70**, 1897-1913, doi:10.1007/s00018-012-1144-9 (2013).

43 Laufer, J. M. *et al.* Chemokine Receptor CCR7 Triggers an Endomembrane Signaling Complex for Spatial Rac Activation. *Cell Rep* **29**, 995-1009 e1006, doi:10.1016/j.celrep.2019.09.031 (2019).

44 Tebar, F., Enrich, C., Rentero, C. & Grewal, T. GTPases Rac1 and Ras Signaling from Endosomes. *Prog Mol Subcell Biol* **57**, 65-105, doi:10.1007/978-3-319-96704-2_3 (2018).

45 Hjorto, G. M. *et al.* Differential CCR7 Targeting in Dendritic Cells by Three Naturally Occurring CC-Chemokines. *Front Immunol* **7**, 568, doi:10.3389/fimmu.2016.00568 (2016).

46 Ricart, B. G., John, B., Lee, D., Hunter, C. A. & Hammer, D. A. Dendritic cells distinguish individual chemokine signals through CCR7 and CXCR4. *J Immunol* **186**, 53-61, doi:10.4049/jimmunol.1002358 (2011).

47 Jorgensen, A. S. *et al.* CCL19 with CCL21-tail displays enhanced glycosaminoglycan binding with retained chemotactic potency in dendritic cells. *J Leukoc Biol* **104**, 401-411, doi:10.1002/JLB.2VMA0118-008R (2018).

48 Xiao, Y. *et al.* A novel significance score for gene selection and ranking. *Bioinformatics* **30**, 801-807, doi:10.1093/bioinformatics/btr671 (2014).

49 Zimmerman, B. *et al.* Differential beta-arrestin-dependent conformational signaling and cellular responses revealed by angiotensin analogs. *Sci Signal* **5**, ra33, doi:10.1126/scisignal.2002522 (2012).

50 Inoue, A. *et al.* Illuminating G-Protein-Coupling Selectivity of GPCRs. *Cell* **177**, 1933-1947 e1925, doi:10.1016/j.cell.2019.04.044 (2019).

51 Leng, W. *et al.* Novel split-luciferase-based genetically encoded biosensors for noninvasive visualization of Rho GTPases. *PLoS One* **8**, e62230, doi:10.1371/journal.pone.0062230 (2013).

52 Schindelin, J. *et al.* Fiji: an open-source platform for biological-image analysis. *Nat Methods* **9**, 676-682, doi:10.1038/nmeth.2019 (2012).

53 Hughes, C. S. *et al.* Single-pot, solid-phase-enhanced sample preparation for proteomics experiments. *Nat Protoc* **14**, 68-85, doi:10.1038/s41596-018-0082-x (2019).

Figure legends

Figure 1. CCR7-stimulated $G_{i/o}$ signaling, βarr recruitment, and receptor internalization. (A) HEK293-CCR7 cells transiently expressing the real-time cAMP sensor CAMYEL were challenged with 10 μM forskolin (or vehicle buffer) to increase cAMP production. 5 min later, the cells were stimulated with 100 nM CCL19, 100 nM CCL21, or vehicle buffer, and inhibition of cAMP production was followed as an indirect measurement of $G_{i/o}$ activation. Area under the curve (AUC) was used to calculate the total cAMP for each chemokine ligand. Data represent the mean ± SE of N=3-4 experiments, and one-way ANOVA with Turkey's multiple comparison post hoc test was performed to determine statistical differences between forskolin and chemokine-stimulated cells (***$p < 0.001$; ****$p < 0.0001$). (B) Schematic representation of the experimental design used to monitor EbBRET between RlucII-βarr1/2 and rGFP-CAAX or rGFP-Rab5 upon CCL19 or CCL21 stimulation of CCR7. (C) EbBRET signal between RlucII-βarr1 recruitment to plasma membrane-anchored rGFP-CAAX or early endosome-anchored rGFP-Rab5 in response to 100 nM CCL19, 100 nM CCL21, or vehicle control stimulation. Data represent the mean ± SE of N=5 experiments, and two-way ANOVA with Turkey's multiple comparison post hoc test was performed to determine statistical differences between the distinct conditions (*$p < 0.05$; **$p < 0.01$; ***$p<0.001$). (D) EbBRET signal between RlucII-βarr2 recruitment to plasma membrane-anchored rGFP-CAAX or early endosome-anchored rGFP-Rab5 in response to 100 nM CCL19, 100 nM CCL21, or vehicle control stimulation. Data represent the mean ± SE of N=5 experiments, and two-way ANOVA with Turkey's multiple comparison post hoc test was performed to determine statistical differences between the distinct conditions (*$p < 0.05$; **$p < 0.01$; ***$p < 0.001$).

Figure 2. CCR7-mediated 'megaplex' formation. (A) Schematic illustration of the working hypothesis. CCR7-mediated G protein signaling does not appear to be affected by βarr recruitment or receptor internalization. Therefore, we hypothesized that CCR7 associates and internalizes with βarr in the 'tail' conformation where βarr does not block the G protein-binding site within CCR7. As this site is available, CCR7 can interact simultaneously with G protein and βarr to form a 'megaplex', which enables the receptor to stimulate G proteins while being internalized into endosomes. (B) EbBRET signal between RlucII-βarr1 (WT or ΔFL) recruitment to plasma membrane-anchored rGFP-CAAX in response to 100 nM CCL19, 100 nM CCL21, or vehicle control stimulation. Data represent the mean ± SE of N=5 experiments, and two-way ANOVA with Turkey's multiple comparison post hoc test was performed to determine statistical differences between the distinct chemokine-stimulation conditions for RlucII-βarr1ΔFL (*$p < 0.05$; **$p < 0.01$) and differences between RlucII-βarr1 and RlucII-βarr1ΔFL within each of the stimulation conditions ($^{\#\#\#\#}p < 0.0001$). (C) EbBRET signal between RlucII-βarr1 (WT or ΔFL) recruitment to endosomally-anchored rGFP-Rab5 in response to 100 nM CCL19, 100 nM CCL21, or vehicle control stimulation. Data represent the mean ± SE of N=5 experiments, and two-way ANOVA with Turkey's multiple comparison post hoc test was performed to determine statistical differences between the distinct chemokine-stimulation conditions for RlucII-βarr1ΔFL (*$p < 0.05$; **$p < 0.01$) and differences between RlucII-βarr1 and RlucII-βarr1ΔFL within each of the stimulation conditions ($^{\#\#\#\#}p < 0.0001$). (D) Schematic representation of the experimental design used to monitor luminescence upon proximity between SmBiT-βarr1 and LgBiT-miniG protein in response to CCR activation. (E) Change in luminescence measured upon stimulation of HEK293-CCR7 cells expressing SmBiT-βarr1 and LgBiT-miniGi in response to 100 nM CCL19 or 100 nM

CCL21 stimulation. The response to CCL19 and CCL21 was in both cases normalized to vehicle control. Data represent the mean ± SE of N=3 experiments, and one-way ANOVA with Turkey's multiple comparison post hoc test was performed to determine statistical differences between the distinct treatments (*$p < 0.05$; **$p < 0.01$; ***$p < 0.001$). (F) Confocal microscopy imaging displaying HEK293 cells co-expressing, CCR7, βarr2-Strawberry and Halo-miniGi protein. In the experiment the cells were treated with either 100 nM CCL19, 100 nM CCL21, or vehicle control for 30 min.

Figure 3. Endosomal $G_{i/o}$ activation by internalized CCR7. (A) Confocal microscopy imaging displaying HEK293-CCR7 cells transiently expressing the early endosomal marker Rab5a-RFP. The cells were treated with either 100 nM CCL19-Alexa488, 100 nM CCL21-Alexa488, or Ni-NTA-Alexa488 for 15 min followed by extensive washout to remove extracellular chemokines. The cells were imaged 15-30 min after this washout step. (B) Schematic representation of the EbBRET-based assay to monitor proximity between RlucII-miniGi and the endosomal marker rGFP-Rab5 upon CCR7 activation from endosomes. (C) EbBRET measurements from CCR7-expressing HEK293 cells co-transfected with RlucII-miniGi and rGFP-Rab5 upon stimulation with 100 nM CCL19, 100 nM CCL21, or vehicle control. Data represents the mean ± SE from N=3 independent experiments. One-way ANOVA with Turkey's multiple comparison post hoc test was applied to determine statistical differences between the measurements (**$p < 0.01$; ***$p < 0.001$). (D) Confocal microscopy imaging displaying CCR7-expressing HEK293 cells co-transfected with the plasma membrane marker RFP-Lck and Halo-miniGi. The cells were stimulated with 100 nM CCL19, 100 nM CCL21, or vehicle control for 10 min. (E) Confocal microscopy imaging displaying CCR7-expressing HEK293 cells co-transfected with the endosomal marker RFP-EEA1 and Halo-miniGi. The cells were stimulated with 100 nM CCL19, 100 nM CCL21, or vehicle control for 30 min.

Figure 4. APEX2-mediated biotinylation of proteins in proximity of CCR7. (A) Schematic illustration of the workflow behind CCR7-APEX2-mediated biotinylation created with BioRender.com. First, the cells are loaded with biotin-tyramide (biotin-T) followed by stimulation of CCR7 by 100 nM CCL19 or CCL21 for 0 min, 2 min, 10 min, or 25 min. For the last 1 min of chemokine-stimulation hydrogen peroxide is added, which initiates the APEX2-mediated oxidation of biotin-tyramide into highly reactive and short-lived radicals. These radicals bind to and thus biotinylate proteins within close proximity to the APEX2 enzyme (~20nm), and thus, label proteins that are in complex with or in close proximity chemokine-stimulated CCR7. Next, the cells are lysed and the resulting biotinylated proteins are captured on neutravidin (Neu) beads followed by extensive washing. Finally, all biotin-labeled proteins are eluted, identified, and analyzed by LC-MS. (B) Western blot analysis of HEK293-CCR7-APEX2 cell lysates, which shows that the biotinylation only takes place in the presence of both biotin-tyramide and hydrogen peroxide. Biotinylated proteins were detected using streptavidin-alexa488. (C) Silver staining of the pull-down experiments demonstrating that the enrichment of biotinylated proteins using neutravidin-coated beads is highly specific. In the control sample, the bound fraction only displays neutravidin band on the SDS-PAGE, whereas the labeled sample shows multiples bands of biotinylated proteins.

Figure 5. Identification of enrichment in proximal proteome of CCR7 following agonist stimulation. (A) Heatmap visualizing select proteins with significant increase ($p < 0.05$ and Log_2

fold-increase > 1) in the proximal proteome of CCR7 for at least one timepoint following chemokine stimulation. The proteins are clustered according to their function with corresponding significance score, which was calculated by combining the absolute value of Log_2 fold-change and -Log10 *p* value as previously suggested[48]. (B) Schematic representation showing organelle markers fused to APEX2 used for spatial controls. (C) Confocal microscope images of HEK293-CCR7 cells expressing each of the organelle markers (PM-APEX2, ENDO-APEX2, and CYTO-APEX2) at their respective subcellular locations. (D) Volcano plots of enrichment differences of PM vs CYTO, ENDO vs PM, and ENDO vs CYTO, respectively. Proteins represented as red dots are significant in PM-CYTO/ENDO-PM pair for plasma membrane protein, and in ENDO-CYTO/ENDO-PM pair for endosomal proteins. (E) Schematic illustration showing the roles of RhoGAP, RhoGEF, and RhoGDI in regulation of the family of Rho-GTPase function. (F) Differential enrichment of RhoGAP, RhoGEF, RhoGDI and other proteins that regulate Rho-GTPase signaling with significant change in the CCR7 proximal proteome following chemokine stimulation. (G) Interaction network of RhoGAP, RhoGEF, and RhoGDI proteins with significant change in the CCR7 proximal proteome following chemokine stimulation.

Figure 6. Compartmentalized CCR7 signaling and regulation of RhoA and Rac1 signaling. (A) Schematic description of the RhoA/Rac1 NanoBiT assay. (B) Change in luminescence measured upon stimulation of HEK293-CCR7 cells expressing SmBiT-PKN1 and LgBiT-RhoA in response to 100 nM CCL19 or 100 nM CCL21 stimulation. The response to CCL19 and CCL21 was in both cases normalized to vehicle control. Data represent the mean ± SE of N=4 experiments, and student's *t* test was performed to determine statistical differences between the distinct chemokine treatments. (C) Change in luminescence measured upon stimulation of HEK293-CCR7 cells expressing SmBiT-Rac1 and LgBiT-PAK1 in response to 100 nM CCL19 or 100 nM CCL21 stimulation. The response to CCL19 and CCL21 was in both cases normalized to vehicle control. Data represent the mean ± SE of N=6 experiments, and student's *t* test was performed to determine statistical differences between the distinct chemokine treatments (**$p < 0.01$). (D) Change in luminescence measured upon stimulation of HEK293-CCR7 cells expressing SmBiT-Cdc42 and LgBiT-WAS1 in response to 100 nM CCL19 or 100 nM CCL21 stimulation. The response to CCL19 and CCL21 was in both cases normalized to vehicle control. Data represent the mean ± SE of N=5 experiments, and student's *t* test was performed to determine statistical differences between the distinct chemokine treatments. (E) Change in luminescence measured upon stimulation of HEK293-CCR7 cells expressing SmBiT-Rac1 and LgBiT-PAK1 in response to 100 nM CCL19 or 100 nM CCL21 stimulation. The cells were either pre-treated with 100 ng/ml PTX for 16 h or control buffer. The response to CCL19 and CCL21 was in both cases normalized to vehicle control. Data represent the mean ± SE of N=4-6 experiments, and one-way ANOVA with Turkey's multiple comparison post hoc test was performed to determine statistical differences between the distinct treatments (****$p < 0.0001$). (F) Change in luminescence measured upon stimulation of HEK293-CCR7 cells expressing SmBiT-Rac1 and LgBiT-PAK1 in response to 100 nM CCL19 or 100 nM CCL21 stimulation. The cells were pre-treated with 30 μM of the endocytosis inhibitor Dyngo-4a or the inactive Dyngo control compound for 30 min. The response to CCL19 and CCL21 was in both cases normalized to vehicle control. Data represent the mean ± SE of N=4 experiments, and one-way ANOVA with Turkey's multiple comparison post hoc test was performed to determine statistical differences between the distinct treatments (****$p < 0.0001$).

Supplementary Table S1. Schematic overview of the C-terminal tail region of 23 chemokine receptors. Likely phosphorylation sites are underlined in bold, and phosphorylation site clusters are marked in grey.

Extended Data Figure S1. (A) βarr2 recruitment to CCR7 in HEK293 cells upon 100 nM CCL19, 100 nM CCL21 or vehicle control using the DiscovRx assay. Data represent the mean ± SE of N=4 experiments, and one-way ANOVA with Turkey's multiple comparison post hoc test was performed to determine statistical differences between the distinct conditions (*$p < 0.05$; ****$p < 0.0001$). (B) Active βarr2-mediated endocytosis of CCR7 in upon 100 nM CCL19, 100 nM CCL21 or vehicle control using the DiscovRx assay. Data represent the mean ± SE of N=4 experiments, and one-way ANOVA with Turkey's multiple comparison post hoc test was performed to determine statistical differences between the distinct conditions (****$p < 0.0001$).

Extended Data Figure S2. Expression of RlucII-βarr1 (WT or ΔFLR) constructs in HEK293-CCR7 cells expressing either rGFP-CAAX or rGFP-Rab5 was determined by luminescence measurement.

Extended Data Figure S3. Change in luminescence measured upon stimulation of HEK293-CCR7 cells co-expressing SmBiT-βarr1 and either LgBiT-miniGi or LgBiT-miniGs in response to 100 nM CCL19 stimulation. The response to CCL19 was in both cases normalized to vehicle control. Data represent the mean ± SE of N=4 experiments, and one-way ANOVA with Turkey's multiple comparison post hoc test was performed to determine statistical differences between the distinct treatments (***$p < 0.001$; ****$p < 0.0001$).

Extended Data Figure S4. CCR7-APEX2 stimulation of $G_{i/o}$ signaling. HEK293-CCR7-APEX2 cells were challenged with 10 μM forskolin (or vehicle buffer) to increase cAMP production either with or without 100 nM CCL19 followed by cAMP determination using the Cisbio cAMP dynamic assay.

Extended Data Figure S5. Identification of enrichment in proximal proteome of CCR7 following agonist stimulation. (A) Heatmap visualizing select proteins with significant change ($p < 0.05$ and Log_2 fold-change > 1) in the proximal proteome of CCR7 for at least one timepoint following chemokine stimulation. (B) Volcano plots showing changes in CCR7 proximity proteome following agonist stimulation. Total of 5582 proteins were analyzed by Student's t-test against the MS data from the unstimulated samples.

Extended Data Figure S6. Western blot analysis of HEK293 cells transfected with PM-APEX2, ENDO-APEX2, or CYTO-APEX2 shows that the biotinylation only takes place in the presence of both biotin-tyramide and hydrogen peroxide, and that they have different proximity proteome. Biotinylated proteins were detected using streptavidin-alexa488.

Material and Protocols

Reagents

Hank's balanced salt solution (HBSS), forskolin, G418, Ni^{2+}-NTA-ATTO-488, HEPES, NaCl, phosphate saline buffer (PBS) tablets, 3-isobutyl-1-methylxanthine (IBMX), KCl, $MgCl_2$, $NaHCO_3$, NaH_2PO_4, glucose, sodium ascorbate, sodium azide, biotin-tyamide, sodium deoxycholate, Tris-HCl, H_2O_2, sodium dodecyl sulfate (SDS), phenylmethylsulfonyl fluoride (PMSF), ethanol, chloroacetamide (CAA), Tween-20, tris(2-carboxyethyl)phosphine (TCEP), ethylenediaminetetraacetic acid (EDTA), and $CaCl_2$ were all purchased from Sigma-Aldrich. Dulbecco's Modified Eagle's Medium (DMEM) high glucose, Opti-MEM reduced serum/no phenol red, Dulbecco's PBS (DPBS), fetal bovine serum (FBS), penicillin/streptomycin, cell dissociation buffer, 0.05% trypsin, Lipofectamine 3000, 4X Bolt™ LDS sample buffer, zeocin, puromycin, poly-D-lysine (PDL), CellLight™ Early Endosomes-RFP BacMam 2.0, 4–20% SDS-PAGE gels, Streptavidin, Alexa Fluor™ 488 conjugate (streptavidin-Alexa488), and silver stain kit were all purchased from Thermo Fisher Scientific. Coelenterazine h, coelenterazine 400a, and Deep Blue C™ were all purchased from NanoLight Technology. NeutrAvidin™ agarose, paraformaldehyde, and Triton X-100 were purchased from Fisher Scientific. CCL19 was purchased from Chemotactics. CCL21 was purchased from GenScript. His-tagged CCL19 was purchased from Creative Biomart. His-tagged CCL21 was purchased from GeneTex. Trolox was purchased from Millipore. The cAMP d2 dynamic assay kit was purchased from Cisbio. Halo Tag ligand was purchased from Promega. Salmon sperm DNA was purchased from Invitrogen. Linear polyethyleneimine 25K (PEI) was purchased from Polysciences.

Cell culture and stable cell line construction

HEK293 cells were cultured in DMEM high glucose supplemented with 10% (v/v) fetal bovine serum and 100 U/ml penicillin/streptomycin. Cells were incubated at 37°C in 5% CO_2. To generate HEK293 cells stably expressing CCR7 (HEK293-CCR7), cells were transfected with pcDNA3/CCR7[17] or pTwist/CMV/CCR7 using Lipofectamine3000. To generate HEK293 cells stably expressing CCR7-APEX2 (HEK293-CCR7-APEX2), cells were transfected with pTwist/CMV/Puro/CCR7-APEX2 using Lipofectamine 3000. To generate HEK293-CCR7 cells stably expressing Lyn11-GFP-APEX2, 2xFYVE-GFP-APEX2, or GFP-APEX2 (HEK293-CCR7-PM-APEX2, HEK293-CCR7-ENDO-APEX2, or HEK293-CCR7-CYTO-APEX2, respectively), cells were transfected with pcDNA3-PM-APEX2[26], pcDNA3-ENDO-APEX2[26], or pcDNA3-CYTO-APEX2[26] using Lipofectamine 3000. 24 hours after the transfection the medium was changed to fresh medium. 48 hours after the transfection the medium was changed again to fresh medium containing 500 μg/mL G418 (HEK293-CCR7), 2 μg/mL puromycin (HEK293-CCR7-APEX2), 100 μg/ml zeocin (HEK293-CCR7 cells used to generate cell lines stably expressing PM-APEX2, ENDO-APEX2, or CYTO-APEX2), or 100 μg/mL zeocin + 100 μg/mL G418 (HEK293-CCR7-PM-APEX2, HEK293-CCR7-ENDO-APEX2, or HEK293-CCR7-CYTO-APEX2) to initiate selection of stably transfected cells. 3-5 days later cells were detached and diluted ~1000-fold for expansion of individual clones. Functional expression of constructs was verified by fluorescence imaging (PM-APEX2, ENDO-APEX2, or CYTO-APEX2), or CCL19-medtaed inhibition of forskolin-stimulated cAMP production (CCR7 and CCR7-APEX2).

Plasmid constructs

Human CCR7 in pcDNA3 was previously described[17]. Human CCR7 was N-terminally tagged with an influenza hemagglutinin signal sequence followed by a FLAG-tag (MKTIIALSYIFCLVFA + DYKDDDDK) into pTWIST/CMV/Zeo and synthesized by Twist Bioscience. For proximity biotin labelling, CCR7 was N-terminally tagged with an influenza hemagglutinin signal sequence followed by a FLAG-tag, and with APEX2 added to the C-terminus through a flexible linker (GGSGGGGSGGSSSGG) and synthesized into pTwist/CMV/Puro using the EcoRI and NheI restriction sites of the vector by Twist Bioscience. Lyn11-GFP-APEX2 (PM-APEX), 2×FYVE-GFP-APEX2 (ENDO-APEX), and GFP-APEX2 (CYTO-APEX) were a kind gift from Dr. Mark von Zastrow and were designed as plasma membrane, endosomal, and cytosolic spatial references, respectively[26]. The CAMYEL biosensor was previously described[19]. RlucII-βarr1 and RlucII-βarr1-ΔFL were previously described[13]. The RlucII-βarr2 construct (*Renilla* Luciferase II in the carboxy-terminal of βarr2) was built by replacing the GFP10-EPAC sequence from the previously published GFP10-EPAC-RlucII[49] with the coding sequence of human βarr2. The rGFP-CAAX and rGFP-Rab5a are cloned into pcDNA3.1(+) and were previously described[21]. MiniGi[24] (also referred to as miniGsi) and miniGs[24] were N-terminally tagged with a LgBiT[50] through a linker (GGSG), and the LgBiT was N-terminally tagged with a nuclear export signal (MLQNELALKLAGLDINKT) via a linker (GGSG), and synthesized into pTwist/CMV using the NotI and BamHI restriction sites of the vector by Twist Bioscience. Human βarr1 was also N-terminally tagged with SmBiT[50] through a linker (GGSG) synthesized by Twist Bioscience. The RlucII-miniGsi was synthetised by Twist Bioscience. The Venus tag from the NES-venus-mGsi contruct[23] was replaced by a *Renilla* Luciferase II and cloned in pTwistCMV expression vector using HindIII and NheI restriction sites of the vector.The NanoBiT-RhoA sensor comprising the SmBiT-RhoA and the LgBiT-PKN1-GDB constructs was described previously[50]. The NanoBiT-Rac1 sensor comprising the SmBiT-Rac1 and the LgBiT-PAK1-GDB constructs and the NanoBiT-Cdc42 sensor comprising the SmBiT-Cdc42 and the LgBiT-WAS-GDB constructs were generated by replacing firefly luciferase fragments of previously described Rac1 and Cdc42 constructs[51] with the NanoBiT fragments. Specifically, the human Rac1 (residues 2-192) and the GTPase-binding domain (GBD) of the human PAK1 (residues 67-150) were N-terminally fused to SmBiT and LgBiT, respectively, with a 15-amino acid flexible linker (GGSGGGGSGGSSSGG). Similarly, the human Cdc42 (residues 2-191) and the GBD of the human WAS (residues 220-288) were N-terminally fused to SmBiT and LgBiT, respectively, with the flexible linker. Coding sequence for Rac1, PAK1-GDB, Cdc42 and WAS-GBD were human codon-optimized and gene-synthesized by Genscript and inserted into the pCAGGS plasmid using an NEBuilder assembly kit. βarr2-Strawberry[9] was a gift from Prof. Larry Barak (Duke University, USA). Halo-miniGi (also referred to as miniGsi) was kindly provided by Prof. Nevin A. Lambert (Augusta University, USA). RFP-Lck (C-tRFP-Lck cloned into PCMV6-AC-RFP expression vector) and RFP-EEA1 (TagRFP-T-EEA1 cloned into pEGFP-C1 vector) were purchased from Addgene (respectively #RC100049 and #42635).

Transfection

DNA for BRET or confocal imaging experiments to be transfected was combined with salmon sperm DNA to obtain a total of 1 µg DNA/condition. PEI was combined with DNA (3 µg PEI per µg of DNA) and incubated 20 minutes before adding cells at 300,000 cells/mL. 30,000 cells/well were then seeded in white 96-well plates (Greiner) or in 8-well glass bottom chamber slides (Ibidi)

for confocal microscopy and cells were incubated for 48 hours before assay. DNA constructs for NanoBiT experiments were combined as described below and transfected into the cells using Lipofectamine 3000.

CAMYEL real-time cAMP assay

HEK293-CCR7 cells were seeded at a density of 1,000,000 cells per 10-cm dish and were transfected the next day with CAMYEL biosensor[19] (YFP-Epac-Rluc) using Lipofectamine 3000 (Invitrogen). The transfected cells were detached and plated 100 µL per well of a PDL-coated white 96-well Microplate (Falcon) and incubated overnight at 37 °C. The cells were equilibrated in HBSS supplemented with 10 mM HEPES (pH 7.4) at 37°C for 30 minutes. Coelenterazine-h was added at a final concentration of 5 µM before starting the measurement. After establishing a baseline response for 2 minutes, cells were stimulated with forskolin at a final concentration of 10 µM and the response was measured. Five minutes after the forskolin stimulation, CCL19 or CCL21 was added at a final concentration of 100 nM and the luminescence was measured for further 15 minutes. The signal was detected at 550 nm using a CLARIOstar instrument (BMG LabTech).

BRET-based assays

Transfected cells were washed with DPBS and assayed in Tyrode's buffer (137 mM NaCl, 0.9 mM KCl, 1 mM $MgCl_2$, 11.9 mM $NaHCO_3$, 3.6 mM NaH_2PO_4, 25 mM HEPES, 5.5 mM glucose, 1 mM $CaCl_2$, pH 7.4) at 37°C. 100 nM CCL19, or 100 nM CCL21, or vehicle were added to cells and incubated at 37°C for 30 minutes. 5 minutes before reading, Renilla luciferase II (RlucII) substrate (coelenterazine 400a; Deep Blue C™) was added at a final concentration of 2.5 µM. All BRET measurements were performed using a FLUOstar Omega microplate reader (BMG Labtech) with an acceptor filter (515 ± 30 nm) and donor filter (410 ± 80 nm). BRET was calculated by dividing GFP emission by RlucII emission.

DiscoveRx PathHunter β-arrestin assay

The PathHunter protein complementation assay (DiscoveRx) using the PathHunter® HEK 293 CCR7 β-Arrestin cell line was performed according to the manufacturer's protocol using and read for chemiluminescent signaling on a NovoStar plate reader (BMG Labtech). In brief, complementary halves of β-galactosidase were genetically fused to the carboxyl termini of the CCR7 and βarr2. Expressed at the same time, the two fusion proteins serve as a proximity sensor; when βarr2 translocates to active receptor, the β-galactosidase fragments interact to form a functional enzyme, which is detected by a chemoluminescent substrate.

DiscoveRx PathHunter activated GPCR internalization assay

βarr-dependent CCR7 internalization was measured using the PathHunter® CCR7 Activated GPCR Internalization U2OS Cell Line (DiscoveRx). In brief, U2OS cells expressing untagged CCR7 co-express complementary halves of β-galactosidase that are fused to βarr2 and an endosomal marker. Expressed at the same time, the two fusion proteins serve as a proximity sensor; when βarr2 internalizes CCR7 into endosomes, the β-galactosidase fragments interact to form a functional enzyme, which is detected by a chemoluminescent substrate.

NanoBiT assays

The NanoBiT assay measures interaction between two proteins each tagged with a LgBiT and a SmBiT, respectively. Multiple NanoBiT assays were performed between LgBiT-miniG/SmBiT-βarr1, LgBiT-RhoA/SmBiT-PKN1-GDB, LgBiT-PAK1-GBD/SmBiT-Rac1, and LgBiT-WAS1-GDB/SmBiT-Cdc42 to check the interaction between each biosensor pair. All biosensors were transfected into HEK293-CCR7 cells using Lipofectamine 3000. For the LgBiT-miniG/SmBiT-βarr1 and LgBiT-RhoA/SmBiT-PKN1-GDB biosensor pairs, 2,000,000 cells were seeded per well in 6 well plates. 24 hours later, 125 ng/125 ng of LgBiT-miniG/SmBiT-βarr1, or 500 ng/100 ng of LgBiT-RhoA/SmBiT-PKN1-GDB were transfected into the cells. For the LgBiT-PAK1-GBD/SmBiT-Rac1 and LgBiT-WAS1-GDB/SmBiT-Cdc42 biosensor pairs, 500,000 cells were seeded per well in 24 well plates. 24 hours later, 25 ng/125 ng LgBiT-PAK1-GBD/SmBiT-Rac1, or 25 ng/125 ng of and LgBiT-WAS1-GDB/SmBiT-Cdc42 were transfected into the cells. The next day, transfected cells were detached and 100,000 cells/well were plated into a PDL-coated white 96-well Microplate (Falcon) and incubated overnight at 37°C. The cells were equilibrated in Opti-MEM™ at 37°C for 60 minutes. Coelenterazine-h was added at a final concentration of 10 µM before starting the measurement. After establishing a baseline response for 2 minutes, cells were stimulated with CCL19 or CCL21 added at a final concentration of 100 nM and the luminescence was measured for further 20 minutes. The signal was detected at 550 nm using a PHERAstar *FSX* instrument (BMG LabTech).

Confocal microscopy

Confocal microscopy experiments were conducted on CCR7 expressing HEK293 cells co-transfected with Halo-miniGi/βarr2-Strawberry, Halo-miniGi/RFP-Lck, or Halo-miniGi/RFP-EEA1. On the same day as the experiments, Oregon green Halo Tag ligand was added to Halo-miniGi expressing cells at a final concentration of 1 µM in the media and incubated 15 minutes at 37°C. Cells were washed 3 times with media and incubated 30 minutes for the last wash at 37°C. Media was then aspirated, replaced by Tyrode's buffer and 100 nM CCL19, 100 nM CCL21, or vehicle were added and cells incubated for 30 minutes at 37°C. Cells were fixed with 4% paraformaldehyde in PBS for 10 minutes at room temperature, washed with DPBS, incubated 10 minutes in DPBS and then DPBS replaced by Tyrode's buffer. Cells were visualized using a Leica SP8 confocal microscope and analyzed using Leica Application Suite X (LASX).

Co-localization analysis

Co-localization was performed using Imaris software version 9.9.1 (Bitplane, Oxford instruments, Switzerland). Cells were selected using the "surfaces" module and cells containing regions of interest were selected. Channels for each fluorophore within the selected cells were masked to exclude all other cells or noise within the image. The Coloc module was then used to calculate co-localized voxels between the different channels. Thresholds were selected based on levels of intensity. Data are reported as percentage of red volume (red voxels) above the threshold that is co-localized with green volume (green voxels) above the threshold.

Fluorescence-coupled chemokine washout experiment

For the washout experiment of fluorescence-coupled chemokines, HEK293-CCR7 cells in a PDL-coated 35 mm glass bottom dishes (MatTek) were transfected with 40 µL of CellLight™ Early Endosomes-RFP, BacMam 2.0. On the next day, 10 µL of 1 mM Ni^{2+}-NTA-ATTO-488 were pre-mixed with 10 µL of 10 µM His-CCL19 or His-CCL21 in 80 µl of HBSS supplemented with 10

mM HEPES (pH 7.4). Following 30-60 minutes of incubation at room temperature, the mixtures were added to the cells for 15 minutes at 37 °C. Next, cells were washed twice in HBSS supplemented with 10 mM HEPES (pH 7.4), and imaging in culture media 15-30 minutes later using an SP8 confocal microscope with HCX PL APO 63x (NA1.40) oil objective (Leica-Microsystems). Images were processed using Fiji[52].

Cisbio cAMP d2 dynamic assay

On the day of the experiment sub-confluent, stably transfected HEK293-CCR7-APEX2 cells were washed once with DPBS and detached from the cell culture plate using cell dissociation buffer. Cells were centrifuged and resuspended in assay buffer (500 nM IBMX + 20 mM HEPES in HBSS buffer, pH 7.4) at a concentration of 400,000 cells/mL. In a white small volume 384-well plate (Greiner), 5 µL of ligand buffer (500 nM IBMX + 20 µM forskolin + 20 mM HEPES in HBSS buffer, pH 7.4) containing 200 nM CCL19 ligand was mixed with 5 µL of cell suspension. The plate was sealed and incubated at room temperature for 30 minutes. Next, 5 µL of lysis buffer containing 2.5% Eu^{3+}-anti-cAMP antibody was added to each well followed by addition of 5 µL of lysis buffer containing 2.5% cAMP-d2. The plate was incubated for 1 hour at room temperature. The plate was read on an PHERAstar FSX instrument (BMG LabTech) where the wells were excited with light at 340 nm and emission light was measured at 615 nm and 665 nm. The TR-FRET 665 nm/615 nm ratio, which is inversely proportional with the cAMP production, was used in combination with a cAMP standard curve to calculate the cAMP production in the cells.

Western blotting of biotinylated proteins

To confirm correct biotinylation in HEK293-CCR7-APEX2, HEK293-CCR7-PM-APEX2, HEK293-CCR7-ENDO-APEX2, or HEK293-CCR7-CYTO-APEX2 cell lines western blotting was conducted. Briefly, cells were preincubated with 500 µM biotin-tyramide in DMEM supplemented with 10% FBS and 100 µg/mL penicillin/streptomycin for 1 hour at 37 °C. The proximity labeling was initiated by addition of freshly diluted H_2O_2 from a 30% (v/v) stock solution to a final concentration of 1 mM. The culture media was removed exactly 1 minute later, and the cells were washed three times with ice cold quenching buffer (PBS supplemented with 10 mM sodium ascorbate, 10 mM sodium azide, and 5 mM Trolox). The cells were detached by adding 5 mL of the quenching buffer supplemented with 5 mM EDTA and incubating at room temperature for 10 minutes with agitation. Detached cells were transferred to a 15-mL conical tube and centrifuged at 1,000×g at 4°C for 10 minutes to remove the supernatant. The pellet was resuspended in LDS sample buffer and proteins resolved on 4–20% SDS-PAGE gels and western blotted using standard procedures. To label biotinylated proteins on the membrane, streptavidin-Alexa488 was used. Finally, all biotinylated proteins were visualized on an Amersham Typhoon instrument (Cytiva).

Data and statistical analysis

All graphs were generated and analyzed using GraphPad Prism 8 (GraphPad Software). Data are presented as mean ± SEM. Differences were assessed using Student's *t* test for two comparisons and one- or two-way ANOVA and Tukey's post hoc test for multiple comparisons. $P < 0.05$ was considered significant at the 95% confidence level.

APEX2 labeling

HEK293 cells transfected with sfhCCR7-APEX2 on 10 cm culture dishes were preincubated with 500 µM biotin-tyramide in DMEM supplemented with 10% FBS and 100 µg/mL penicillin/streptomycin for one hour at 37 °C. Recombinant human CCL19 or CCL21 were added to 100 nM during the incubation so that the cells are stimulated for 2, 10, or 25 minutes respectively, at the end of the one-hour biotin-tyramide incubation period. The proximity labeling is initiated by addition of freshly diluted H_2O_2 from a 30% (v/v) stock solution to a final concentration of 1 mM. The culture media was removed exactly 1 minute later, and the cells were washed three times with ice cold quenching buffer (PBS supplemented with 10 mM sodium ascorbate, 10 mM sodium azide, and 5 mM Trolox). The cells were detached by adding 5 mL of the quenching buffer supplemented with 5 mM EDTA and incubating at room temperature for 10 minutes with agitation. Detached cells were transferred to a 15-mL conical tube and centrifuged at 1,000×g at 4°C for 10 minutes to remove the supernatant. The pellet was stored at -80°C until cell lysis.

The frozen cell pellet was lysed with 1 mL RIPA buffer (50 mM Tris-HCl, 150 mM NaCl, 1% Triton X-100, 0.5% sodium deoxycholate, 0.1% SDS, pH 7.4) supplemented with 1 mM PMSF for 30 minutes at room temperature with agitation. The cell lysate was further solubilized by brief sonication and centrifuged at 12,000×g at 4°C for 10 minutes to remove any insoluble cell debris. NeutrAvidin™ agarose beads were pre-washed three times with 20 bed volumes of the RIPA buffer and incubated with the supernatant overnight at 4°C with agitation. After the incubation, the beads were washed by incubating at room temperature for 10 minutes each with 40 bed volumes of buffer A (2% SDS), buffer B (50 mM HEPES, 500 mM NaCl, 1 mM EDTA, 1% Triton X-100, 0.1% sodium deoxycholate, pH 7.4), then buffer C (10 mM Tris-HCl, 500 mM NaCl, 1 mM EDTA, 0.1% Tween-20, 0.5% sodium deoxycholate, pH 8.0) with agitation. The beads were further washed twice with 20 bed volumes of 100 mM HEPES (pH 7.4) and once with PBS (pH 7.4) to remove trace amount of detergent. Washed beads were resuspended in 100 µL PBS and subjected to mass spectrometry analysis. To follow the enrichment of biotinylated proteins during this procedure, small samples at each step were collected and assessed by SDS-PAGE and silver staining.

Mass spectrometry and data acquisition

Proteins on the NeutrAvidin™ agarose beads were eluted by incubating with 50 µL of 50 mM Tris-HCl, 5% SDS, 10 mM TCEP, 20 mM CAA (pH 7.4) at 90°C for 20 minutes. Eluted proteins were purified and digested on magnetic beads following SP3 workflow[53]. Eluates were transferred into clean Eppendorf tubes and mixed with SP3 magnetic beads. Proteins were precipitated by mixing with equal volume of ethanol and SP3 beads were washed three times with 200 µL of 85% ethanol to remove any traces of SDS from the elution buffer. The SP3 beads were suspended in 50 µL of 50 mM Tris-HCl (pH 7.4) and the proteins on the beads were digested with trypsin (4 ng/µL) at 37°C overnight. Trypsin digestion was quenched by adding TFA to a final concentration of 0.5%. Peptide digests were transferred from the magnetic beads into the clean tubes. SP3 beads were washed with 50 uL of 5% ACN 0.2% TFA. The peptides were loaded on Evotips C18 (Evosep) for subsequent LC-MS/MS analysis using Evosep One LC system coupled to Q Exactive™ HF-X Hybrid Quadrupole-Orbitrap™ MS instrument (Thermo Scientific) operating in data-independent acquisition mode (DIA). Peptides were separated online utilizing 15SPD method (88 min LC gradient length). High resolution full MS1 spectra were acquired with a resolution of 120,000, automatic gain control (AGC) target at 3,000,000 and maximum ion injection time at 60

ms, with a scan range of 350–1,650 m/z. Following each full MS1 scan, 22 data-independent high energy collisional dissociation (HCD) MS/MS scans were acquired at the resolution of 30,000, AGC target of 3,000,000 with stepped normalized collision energy (NCE) of 22.5, 25, and 27.5 Collected DIA data were analyzed using Spectronaut software (Biognosis; https://biognosys.com/shop/spectronaut) and searched in directDIA mode against the SwissProt subset of the human UniProt database (http://www.uniprot.org/). Database search was performed in integrated search engine Pulsar (Biognosis). For the database search, the enzyme specificity was set to trypsin with the maximum number of missed cleavages allowed set to two. Oxidation of methionine was searched as variable modification, whereas carbamidomethylation of cysteines was searched as a fixed modification. The false discovery rate (FDR) for peptide, protein, and site identification was set to 1%. Protein quantification was performed on MS2 level using 3 most intense fragment ions per precursor. Proteins identified with a single peptide was removed from further analysis. The mass spectrometry raw files are accessible under MassIVE ID: MSV000090362 at https://massive.ucsd.edu. Subsequent data analysis steps were performed in Perseus and GraphPad Prism.

Statistical analysis of the MS data

For spatiotemporal characterization of CCR7 upon agonist stimulation, global median normalization was performed for dataset from each time points (0, 2, 10, and 25 minutes after agonist stimulation). Pairwise differential expression analysis was performed by comparing the stimulated datasets (2, 10, and 25 minutes) to the unstimulated (0 minute) dataset using t-test model, assuming equal variance for each protein being compared. For each stimulated time point, proteins with p value < 0.05 and $\log_2$(fold-change) > 1 were considered significant. Significance score for the proteins were calculated by taking the absolute value of the $\log_2$(fold-change) and adding -$\log_{10}$(p value).

Proteins with relevance to Rho, Rac, or CDC42 were selected manually from the list and subjected to further analysis for the role of CCR7 in cell motility. These proteins were searched on the STRING database to build a network functional relevance.

For spatial references PM-APEX2, ENDO-APEX2, and CYTO-APEX2, global median normalization was also performed. Pairwise differential expression analysis between each pair (ENDO against PM, ENDO against CYTO, and PM against CYTO) were performed as above. For each comparison pair, proteins with p value < 0.05 and $\log_2$(fold-change) > 1 were considered significant. Then, proteins commonly appear significant for ENDO and PM from the t-tests were chosen as spatial references.

Figure 1

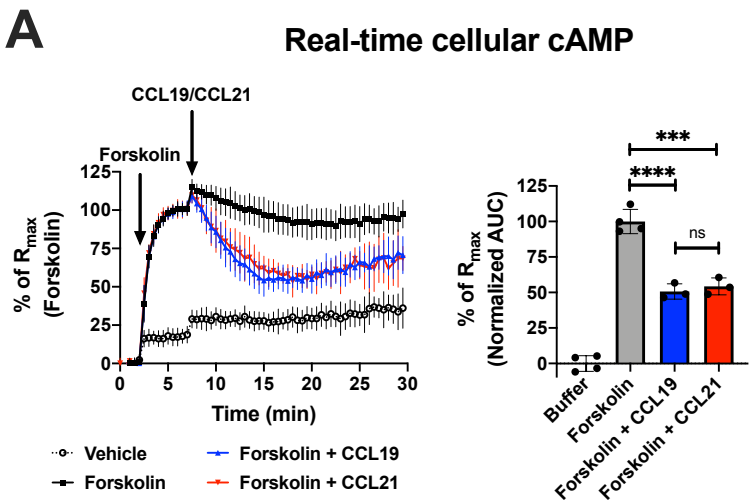
A
Real-time cellular cAMP
CCL19/CCL21
Forskolin
% of Rmax (Forskolin)
Time (min)
Vehicle
Forskolin
Forskolin + CCL19
Forskolin + CCL21
% of Rmax (Normalized AUC)
***
****
ns
Buffer
Forskolin
Forskolin + CCL19
Forskolin + CCL21

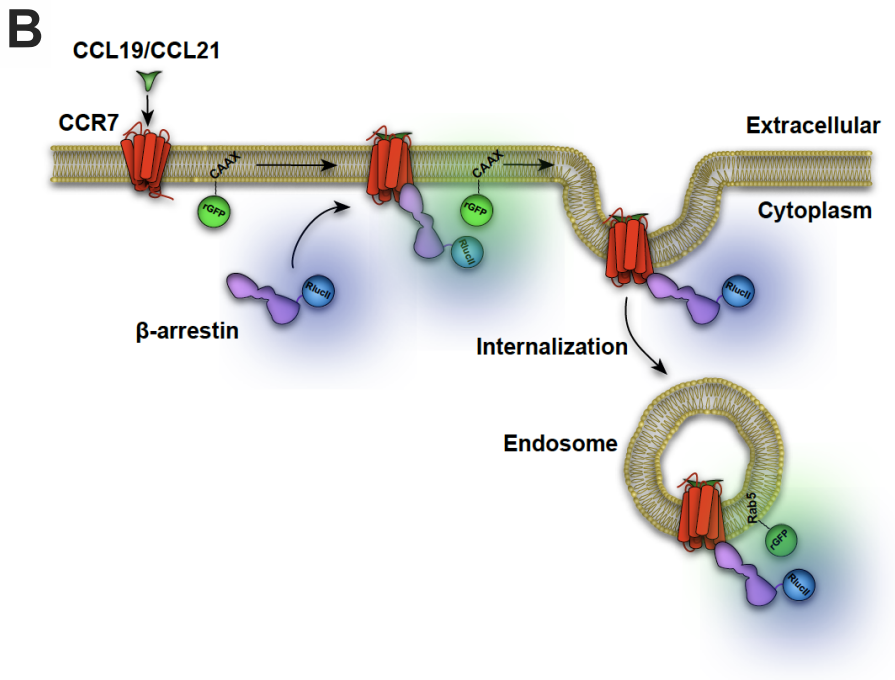
B
CCL19/CCL21
CCR7
Extracellular
Cytoplasm
CAAX
rGFP
RlucII
β-arrestin
Internalization
Endosome
Rab5

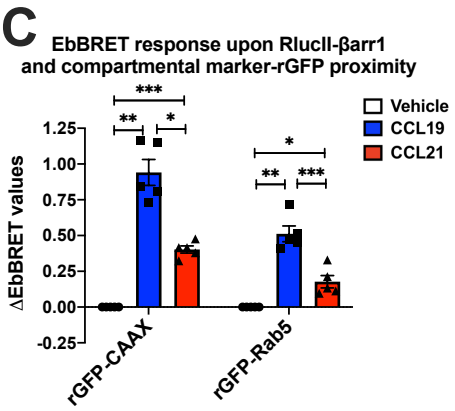
C
EbBRET response upon RlucII-βarr1 and compartmental marker-rGFP proximity
Vehicle
CCL19
CCL21
ΔEbBRET values
rGFP-CAAX
rGFP-Rab5

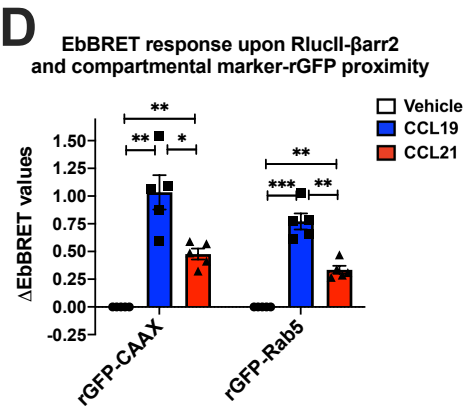
D
EbBRET response upon RlucII-βarr2 and compartmental marker-rGFP proximity
Vehicle
CCL19
CCL21
ΔEbBRET values
rGFP-CAAX
rGFP-Rab5

Figure 2

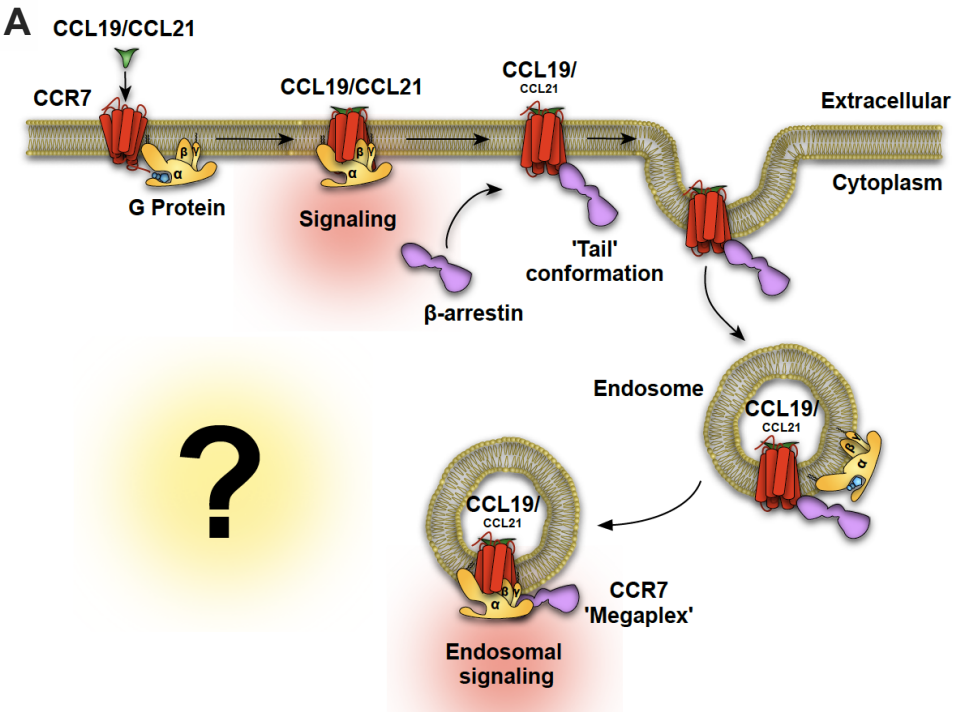
A
CCL19/CCL21
CCR7
G Protein
CCL19/CCL21
Signaling
CCL19/
CCL21
'Tail'
conformation
β-arrestin
Extracellular
Cytoplasm
Endosome
CCL19/
CCL21
?
CCL19/
CCL21
CCR7
'Megaplex'
Endosomal
signaling

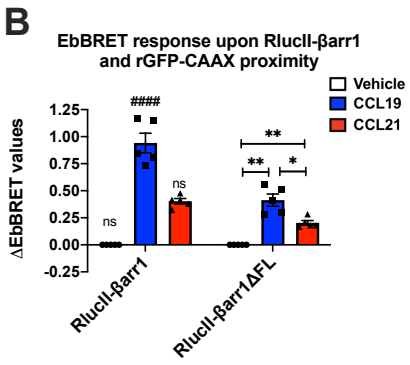
B
EbBRET response upon RlucII-βarr1
and rGFP-CAAX proximity
Vehicle
CCL19
CCL21
ΔEbBRET values
1.25
1.00
0.75
0.50
0.25
0.00
-0.25
####
ns
ns
**
**
*
RlucII-βarr1
RlucII-βarr1ΔFL

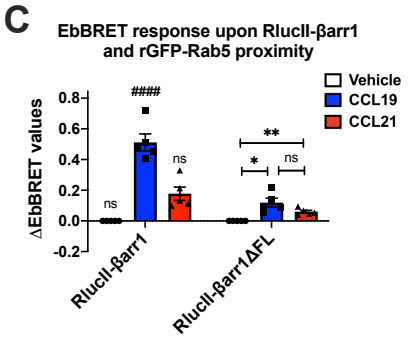
C
EbBRET response upon RlucII-βarr1
and rGFP-Rab5 proximity
Vehicle
CCL19
CCL21
ΔEbBRET values
0.8
0.6
0.4
0.2
0.0
-0.2
####
ns
ns
**
*
ns
RlucII-βarr1
RlucII-βarr1ΔFL

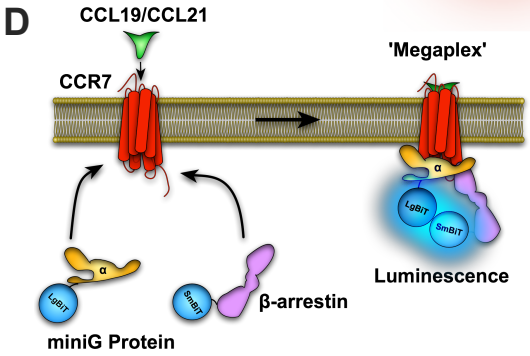
D
CCL19/CCL21
CCR7
'Megaplex'
LgBiT
SmBiT
Luminescence
β-arrestin
miniG Protein

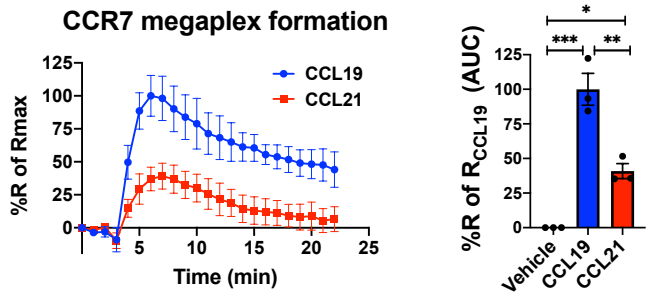
E
CCR7 megaplex formation
CCL19
CCL21
%R of Rmax
125
100
75
50
25
0
5
10
15
20
25
Time (min)
%R of RCCL19 (AUC)
*
***
**
Vehicle
CCL19
CCL21

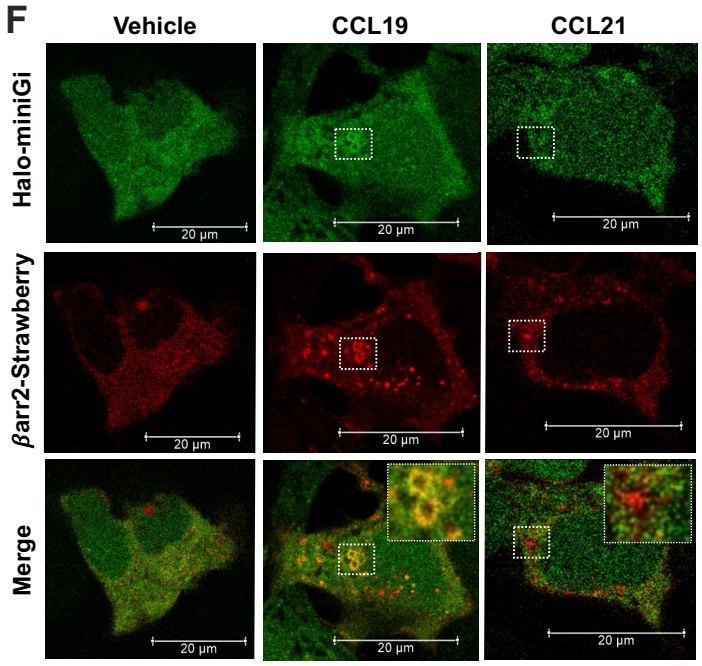
F
Vehicle
CCL19
CCL21
Halo-miniGi
βarr2-Strawberry
Merge
20 μm

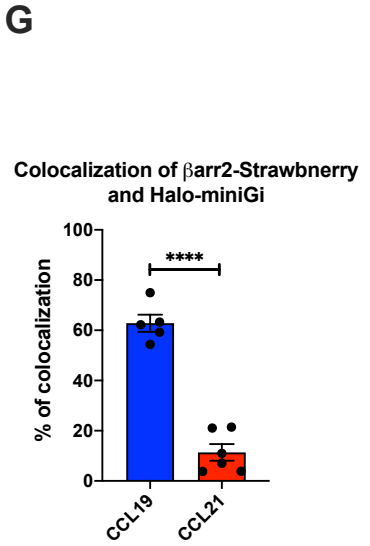
G
Colocalization of βarr2-Strawbnerry
and Halo-miniGi
% of colocalization
100
80
60
40
20
0
****
CCL19
CCL21

Figure 3

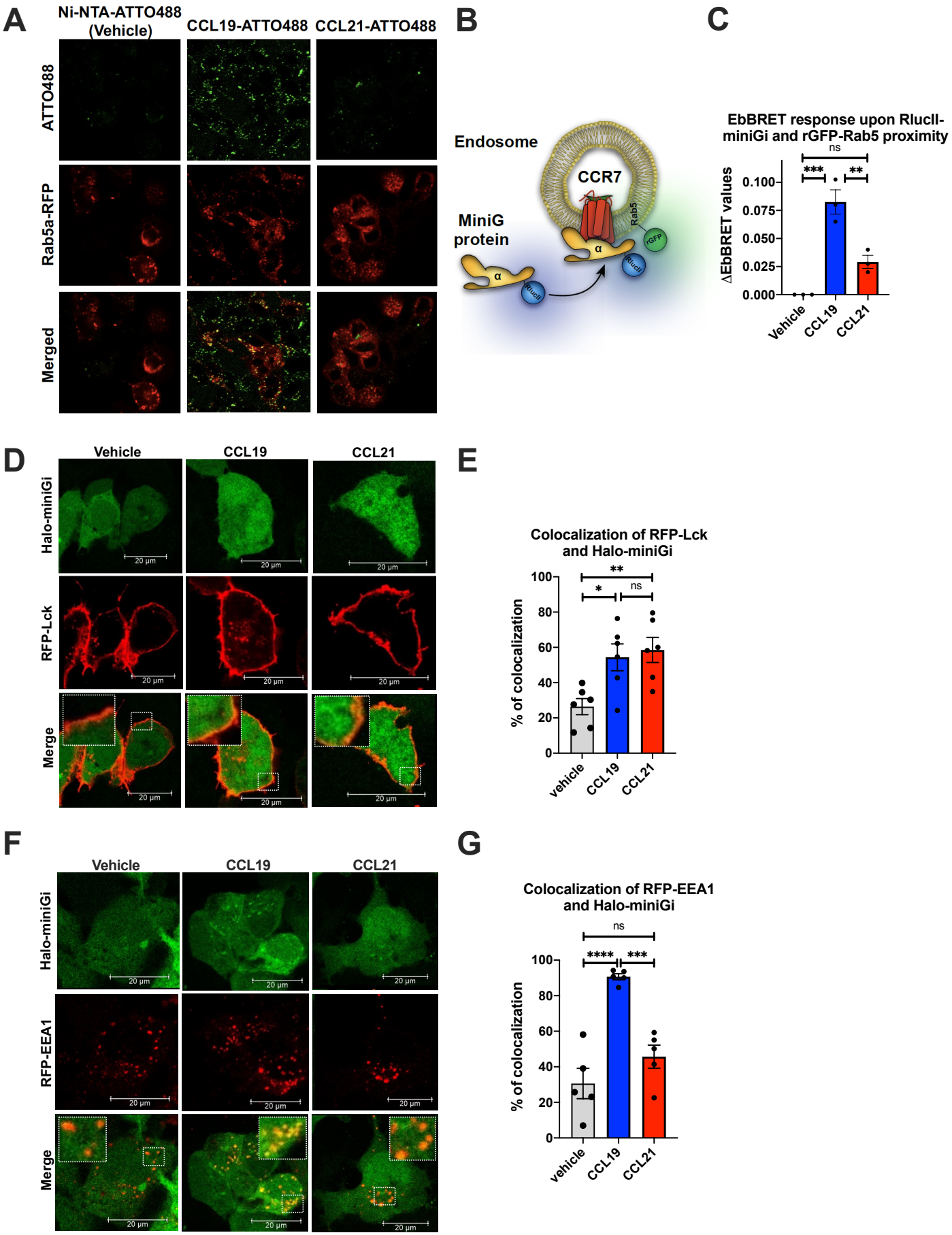
A
Ni-NTA-ATTO488 (Vehicle)
CCL19-ATTO488
CCL21-ATTO488
ATTO488
Rab5a-RFP
Merged
B
Endosome
CCR7
MiniG protein
Rab5
rGFP
RlucII
α
C
EbBRET response upon RlucII-miniGi and rGFP-Rab5 proximity
ΔEbBRET values
ns
***
**
0.100
0.075
0.050
0.025
0.000
Vehicle
CCL19
CCL21
D
Vehicle
CCL19
CCL21
Halo-miniGi
RFP-Lck
Merge
20 µm
E
Colocalization of RFP-Lck and Halo-miniGi
% of colocalization
**
*
ns
100
80
60
40
20
0
vehicle
CCL19
CCL21
F
Vehicle
CCL19
CCL21
Halo-miniGi
RFP-EEA1
Merge
20 µm
G
Colocalization of RFP-EEA1 and Halo-miniGi
% of colocalization
ns
****
***
100
80
60
40
20
0
vehicle
CCL19
CCL21

Figure 4

A

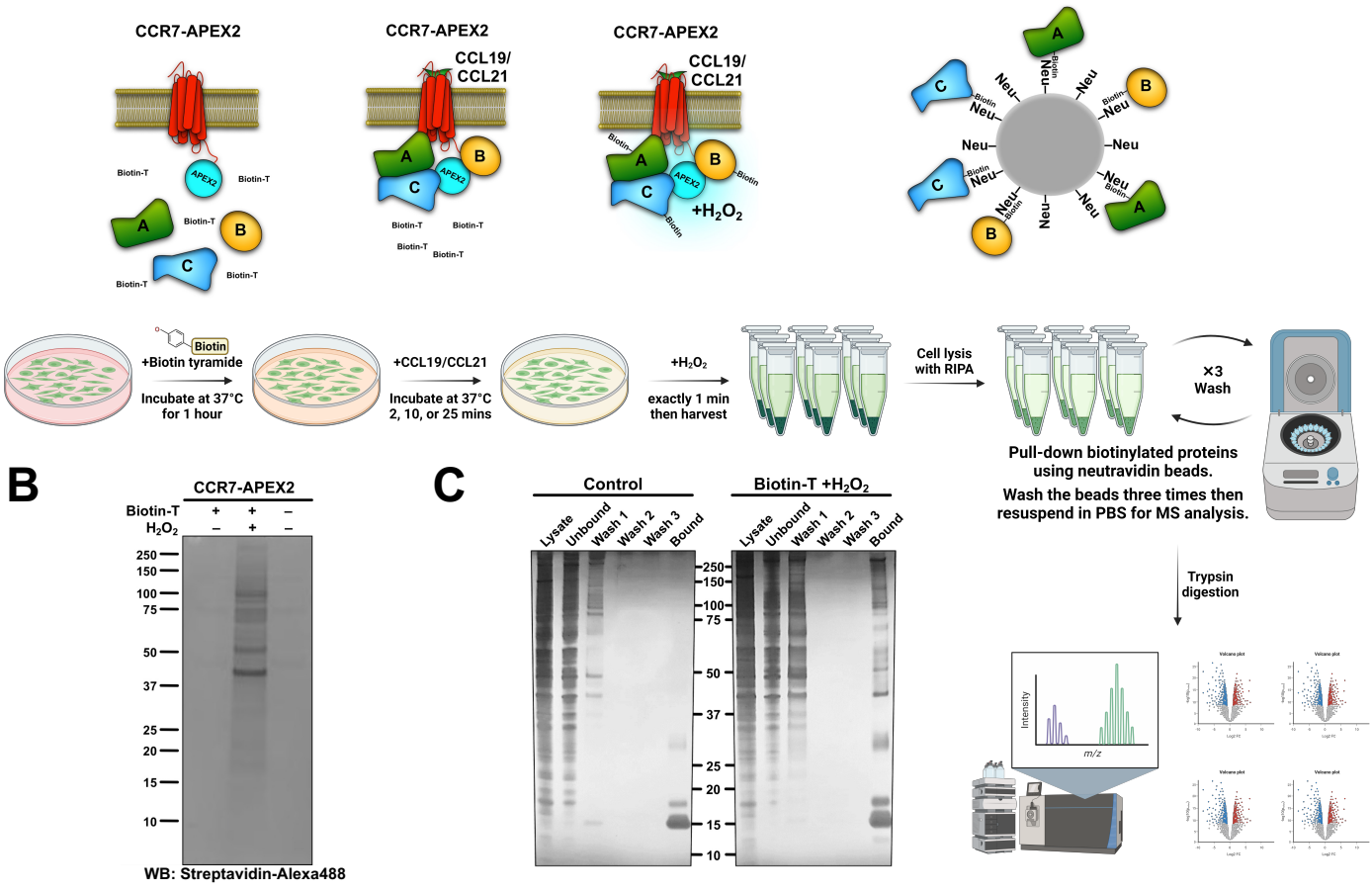
CCR7-APEX2
CCR7-APEX2
CCL19/
CCL21
CCR7-APEX2
CCL19/
CCL21
+H2O2
Biotin-T
APEX2
A
B
C
Neu
Biotin
Biotin
+Biotin tyramide
Incubate at 37°C
for 1 hour
+CCL19/CCL21
Incubate at 37°C
2, 10, or 25 mins
+H2O2
exactly 1 min
then harvest
Cell lysis
with RIPA
×3
Wash
Pull-down biotinylated proteins
using neutravidin beads.
Wash the beads three times then
resuspend in PBS for MS analysis.
Trypsin
digestion
Intensity
m/z

B

CCR7-APEX2
Biotin-T + + –
H2O2 – + –
250
150
100
75
50
37
25
20
15
10
WB: Streptavidin-Alexa488

C

Control
Biotin-T +H2O2
Lysate
Unbound
Wash 1
Wash 2
Wash 3
Bound
250
150
100
75
50
37
25
20
15
10

Figure 5

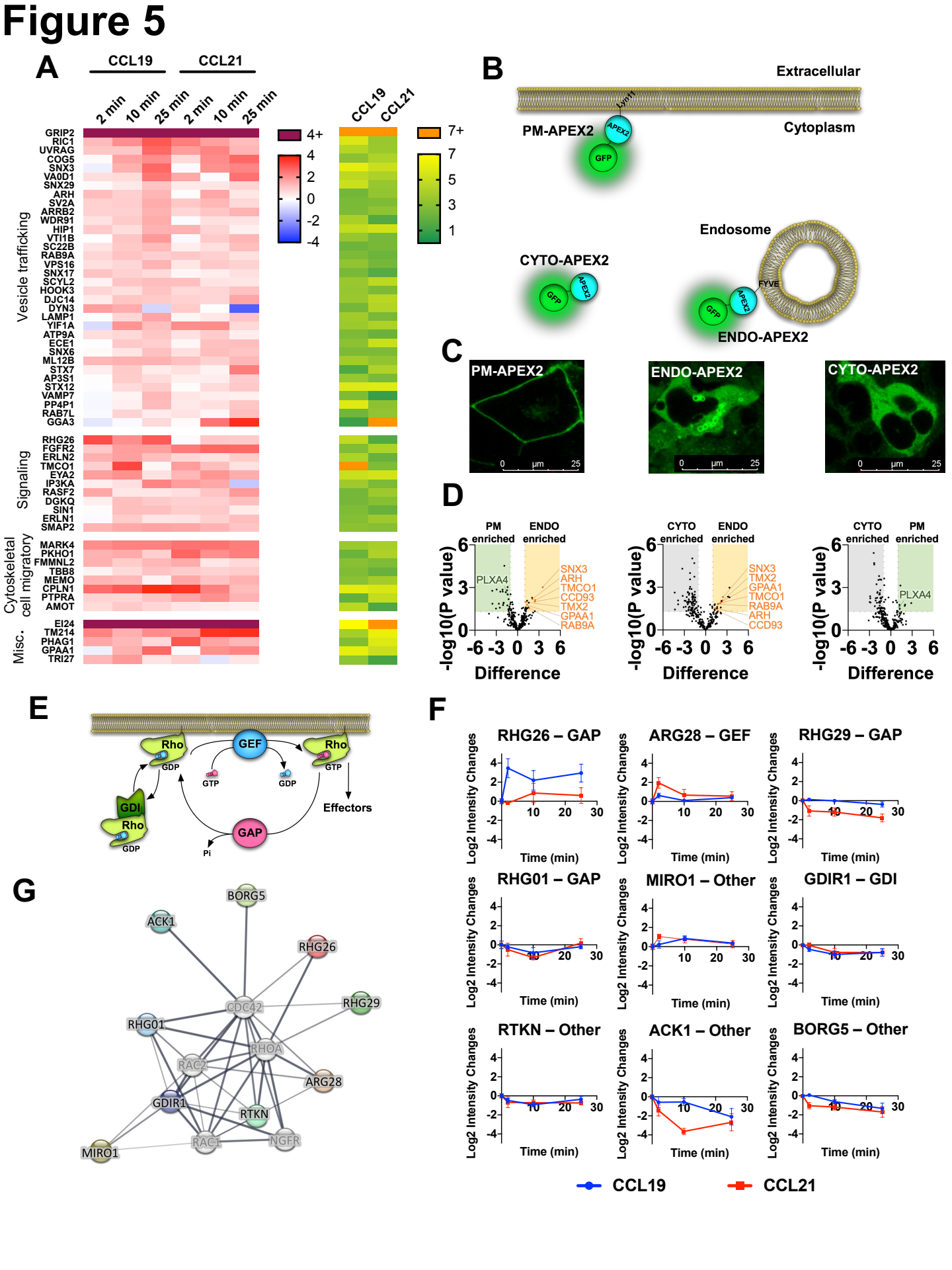
A
CCL19
CCL21
2 min
10 min
25 min
2 min
10 min
25 min
CCL19
CCL21
4+
4
2
0
-2
-4
7+
7
5
3
1
Vesicle trafficking
GRIP2
RIC1
UVRAG
COG5
SNX3
VA0D1
SNX29
ARH
SV2A
ARRB2
WDR91
HIP1
VTI1B
SC22B
RAB9A
VPS16
SNX17
SCYL2
HOOK3
DJC14
DYN3
LAMP1
YIF1A
ATP9A
ECE1
SNX6
ML12B
STX7
AP3S1
STX12
VAMP7
PP4P1
RAB7L
GGA3
Signaling
RHG26
FGFR2
ERLN2
TMCO1
EYA2
IP3KA
RASF2
DGKQ
SIN1
ERLN1
SMAP2
Cytoskeletal cell migratory
MARK4
PKHO1
FMMNL2
TBB8
MEMO
CPLN1
PTPRA
AMOT
Misc.
EI24
TM214
PHAG1
GPAA1
TRI27
B
Extracellular
Cytoplasm
PM-APEX2
APEX2
GFP
CYTO-APEX2
Endosome
FYVE
ENDO-APEX2
C
PM-APEX2
ENDO-APEX2
CYTO-APEX2
0
µm
25
D
PM enriched
ENDO enriched
CYTO enriched
ENDO enriched
CYTO enriched
PM enriched
-log10(P value)
Difference
PLXA4
SNX3
ARH
TMCO1
CCD93
TMX2
GPAA1
RAB9A
TMX2
GPAA1
TMCO1
RAB9A
ARH
CCD93
E
Rho
GDP
GEF
GTP
GDP
Rho
GTP
Effectors
GDI
Rho
GDP
GAP
Pi
F
RHG26 – GAP
ARG28 – GEF
RHG29 – GAP
RHG01 – GAP
MIRO1 – Other
GDIR1 – GDI
RTKN – Other
ACK1 – Other
BORG5 – Other
Log2 Intensity Changes
Time (min)
CCL19
CCL21
G
BORG5
ACK1
RHG26
CDC42
RHG29
RHG01
RHOA
RAC2
ARG28
GDIR1
RTKN
RAC1
NGFR
MIRO1

Figure 6

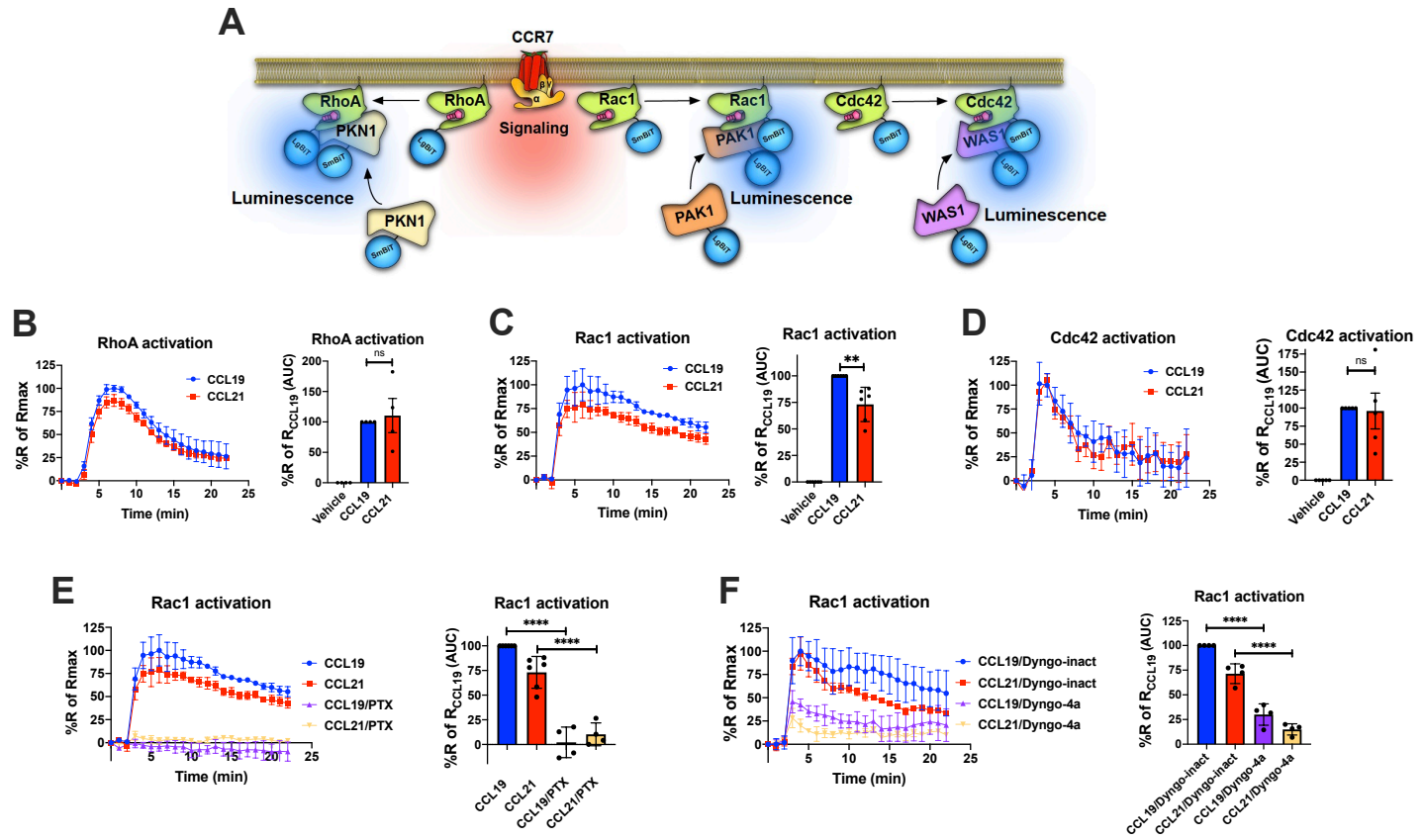
A
CCR7
Signaling
RhoA
PKN1
Rac1
PAK1
Cdc42
WAS1
Luminescence
B
RhoA activation
CCL19
CCL21
Time (min)
%R of Rmax
ns
Vehicle
C
Rac1 activation
**
D
Cdc42 activation
E
CCL19/PTX
CCL21/PTX
****
F
CCL19/Dyngo-inact
CCL21/Dyngo-inact
CCL19/Dyngo-4a
CCL21/Dyngo-4a

Supplementary Table 1

Chemokine receptor	Chemokines	C-terminal tail
CCR1	CCL3, CCL4, CCL5, CCL7, CCL8, CCL13, CCL14, CCL16, CCL23	RVAVHLVKWLPFLSVDRLERVSSTSPSTGEHELSAGF
CCR2	CCL2, CCL7, CCL8, CCL11, CCL13, CCL16, CCL24, CCL26	CRIAPLQKPVCGGPGVRPGKNVKVTTQGLLDGRGKGKSIGRAPEASLQDKEGA
CCR3	CCL2, CCL5, CCL7, CCL8, CCL11, CCL13, CCL15, CCL24, CCL26, CCL28, CXCL9, CXCL10, CXCL11	HLLMHLGRYIPFLPSEKLERTSSVSPSTAEPELSIVF
CCR4	CCL17, CCL22	TCRGLFVLCQYCGLLQIYSADTPSSSYTQSTMDHDLHDAL
CCR5	CCL2, CCL3, CCL4, CCL5, CCL7, CCL8, CCL11, CCL13, CCL14, CCL16	KHIAKRFCKCCSIFQQEAPERASSVYTRSTGEQEISVGL
CCR6	CCL20, β-defensin 4A	CVRRKYKSSGFSCAGRYSENISRQTSETADNDNASSFTM
CCR7	CCL19, CCL21	DLGCLSQEQLRQWSSCRHIRRSSMSVEAETTTTFSP
CCR8	CCL1, CCL8	SCSQIFNYLGRQMPRESCEKSSSCQQHSSRSSSVDYIL
CCR9	CCL25	QWVSFTRREGSLKLSSMLLETTSGALSL
CCR10	CCL27, CCL28	GGSCPSGPQPRRGCPRRPRLSSCSAPTETHSLSWDN
CXCR1	CXCL6, CXCL8	GLVSKEFLARHRVTSYTSSSVNVSSNL
CXCR2	CXCL1, CXCL2, CXCL3, CXCL5, CXCL6, CXCL7, CXCL8	GLISKDSLPKDSRPSFVGSSSGHTSTTL
CXCR3	CCL5, CCL7, CCL11, CCL13, CCL19, CCL20, CXCL9, CXCL10, CXCL11, CXCL12α	GCPNQRGLQRQPSSSRRDSSWSETSEASYSGL
CXCR4	CXCL12, CXCL12α, CXCL12β, CXCL12γ, CXCL12δ, CXCL12ε, CXCL12φ	SVSRGSSLKILSKGKRGGHSSVSTESESSSFHSS
CXCR5	CXCL13	KLGCTGPASLCQLFPSWRRSSLSESENATSLTTF
CXCR6	CXCL16	CLPYLGVSHQWKSSEDNSKTFSASHNVEATSMFQL
GPR35	CXCL17?	VAPSAKAHKSQDSLCVTLA
XCR1	?	FWFCRLQAPSPASIPHSPGAFAYEGASFY
CX_3CR1	CX_3CL1	CLAVLCGRSVHVDFSSSESQRSRHGSVLSSNFTYHTSDGDALLLL
ACKR1	CCL2, CCL5, CCL7, CCL11, CCL14, CCL17, CXCL5, CXCL6, CXCL8, CXCL11	EGWSSHLDTLGSKS
ACKR2	CCL2, CCL3, CCL4, CCL5, CCL7, CCL8, CCL11, CCL13, CCL14, CCL17, CCL22	VLGWHLAPGTAQASLSSCSESSILTAQEEMTGMNDLGERQSENYPNKEDVGNKSA
ACKR3	CXCL11, CXCL12α	YSAKTGLTKLIDASRVSETEYSALEQSTK
ACKR4	CCL19, CCL21, CCL25	RQSVEEFPFDSEGPTEPTSTFSI

Extended Data Figure S1

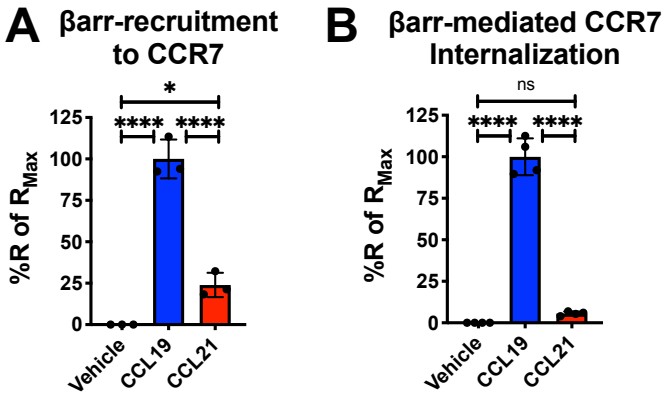

Extended Data Figure S2

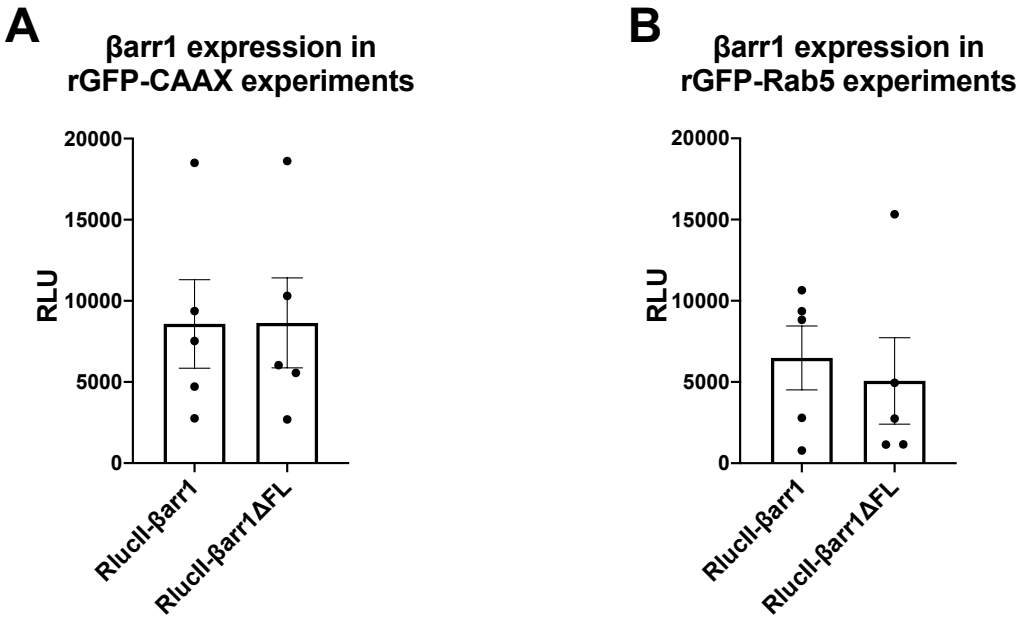

Extended Data Figure S3

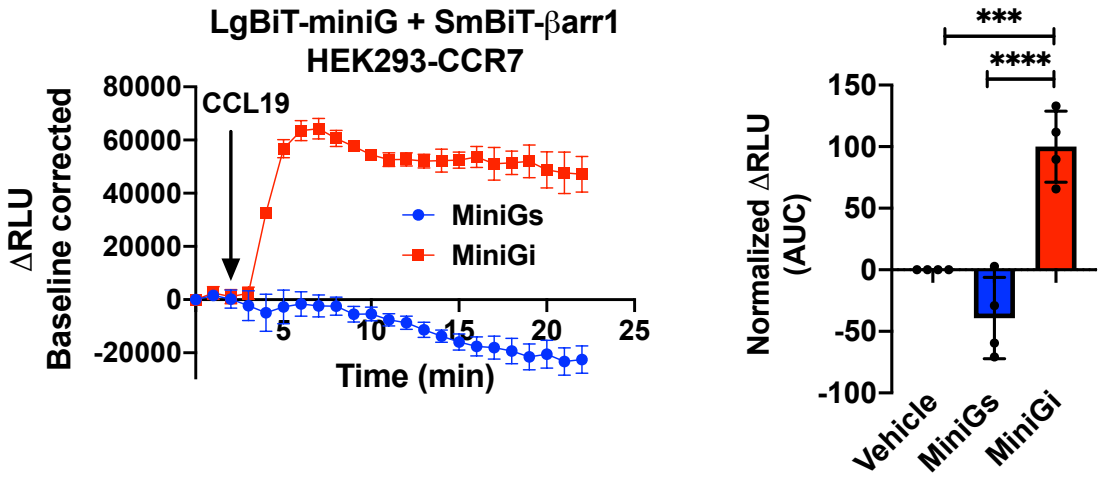

Extended Data Figure S4

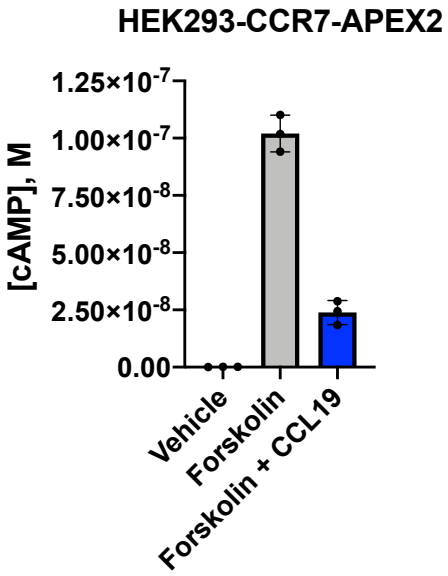

Extended Data Figure S5

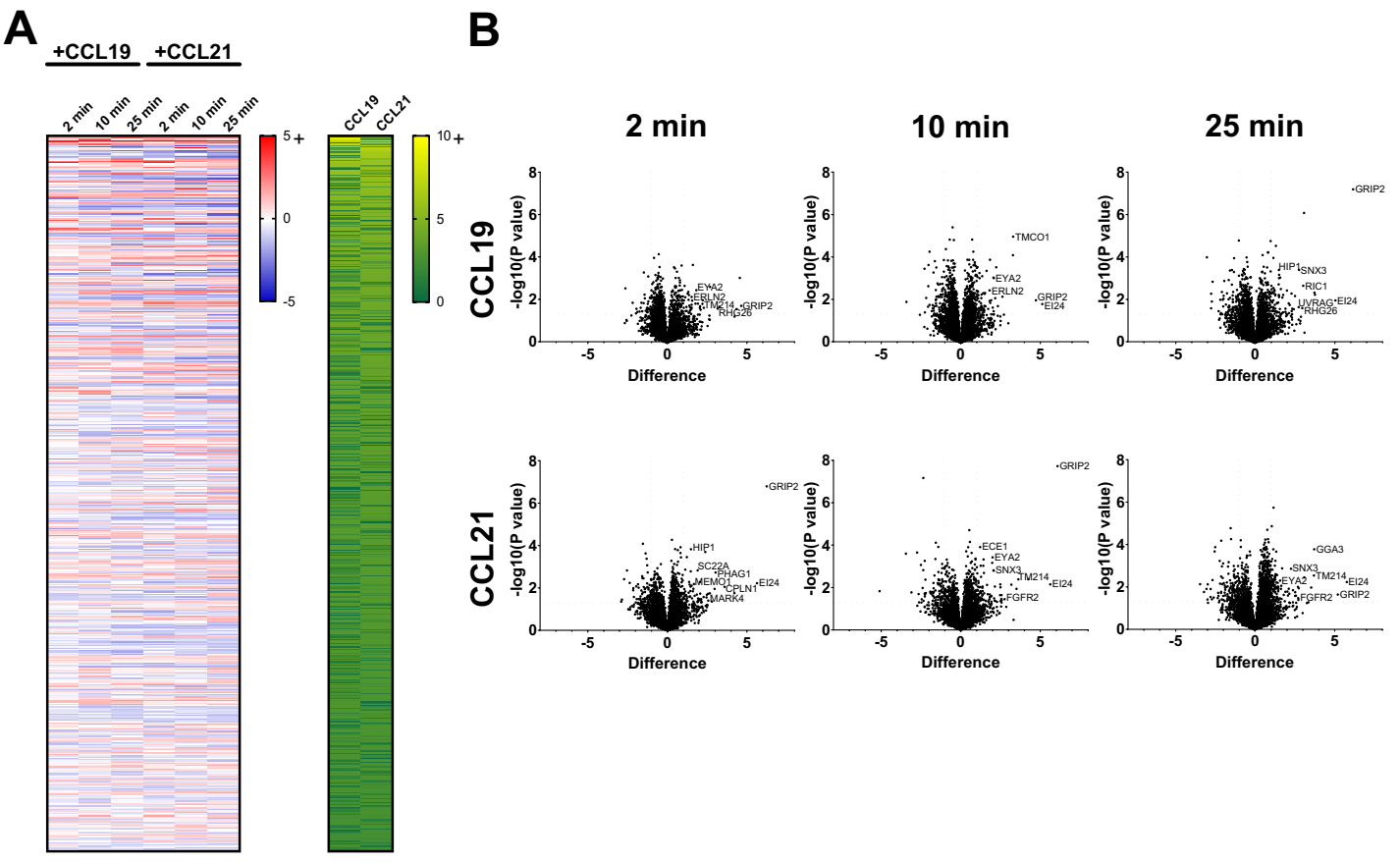

Extended Data Figure S6